Parallel Expansion and Divergence of an Adhesin Family in Pathogenic Yeasts Including *Candida auris*

Rachel A. Smoak[*1], Lindsey F. Snyder[*2], Jan S. Fassler[^3], Bin Z. He[^3]

[1]Civil and Environmental Engineering, [2]Interdisciplinary Graduate Program in Genetics, [3]Biology Department, University of Iowa, Iowa City, IA 52242

*These authors contributed equally

^Correspondence should be addressed to:

Bin Z. He, bin-he@uiowa.edu

Jan S. Fassler: jan-fassler@uiowa.edu

Abstract

Opportunistic yeast pathogens evolved multiple times in the Saccharomycetes class, including the recently emerged, multidrug-resistant *Candida auris*. We show that homologs of a known yeast adhesin family in *Candida albicans*, the Hyr/Iff-like (Hil) family, are enriched in distinct clades of *Candida* species as a result of multiple, independent expansions. Following gene duplication, the tandem repeat-rich region in these proteins diverged extremely rapidly and generated large variations in length and β-aggregation potential, both of which were known to directly affect adhesion. The conserved N-terminal effector domain was predicted to adopt a β-helical fold followed by an α-crystallin domain, making it structurally similar to a group of unrelated bacterial adhesins. Nonsynonymous-to-synonymous substitution rate analysis of the effector domain in *C. auris* revealed relaxed selective constraint and signatures of positive selection, suggesting functional diversification after gene duplication. Lastly, we found the Hil family genes to be enriched at chromosomal ends, which likely contributed to their expansion via ectopic recombination and break-induced replication. We hypothesize that the expansion and diversification of adhesin families are a key step toward the emergence of fungal pathogens and also generate variation in adhesion and virulence within and between species.

Introduction

Candida auris, a newly emerged multidrug-resistant yeast pathogen, is associated with a high mortality rate (up to 60% in a multi-continent meta-analysis (Lockhart et al. 2017)) and has caused multiple outbreaks across the world (CDC global *C. auris* cases count, February 15th, 2021). As a result, it became the first fungal pathogen to be designated by CDC as an urgent threat (CDC 2019). The emergence of *C. auris* as a pathogen is part of a bigger evolutionary puzzle: *Candida* is a polyphyletic genus that contains most of the human yeast pathogens. Phylogenetically, species like *C. albicans*, *C. auris* and *C. glabrata* belong to distinct clades with close relatives that either don't or only rarely infect humans (Fig. 1A). This strongly suggests that the ability to infect humans evolved multiple times in yeasts (Gabaldón et al. 2016). Because many of the newly emerged *Candida* pathogens are either resistant or can quickly evolve resistance to antifungal drugs (Lamoth et al. 2018; Srivastava et al. 2018), it is urgent to understand how yeast pathogenesis arose and what increases their survival in the host. We reason that any shared genetic changes among independently derived *Candida* pathogens will reveal key factors for host adaptation.

Gene duplication and the subsequent functional divergence is a major source for the evolution of novel phenotypes (Zhang 2003; Qian and Zhang 2014; Kuang et al. 2016; Eberlein et al. 2017). In a genome comparison of seven pathogenic *Candida* species and nine low-pathogenic potential relatives, three of the top six pathogen-enriched gene families encode GlycosylPhosphatidylInositol (GPI)-anchored cell wall proteins, namely Hyr/Iff-like, Als-like and Pga30-like (Butler et al. 2009). The first two encode known fungal adhesins (Bailey et al. 1996; Hoyer 2001; Luo et al. 2010). These glycosylated cell wall proteins play key roles in fungal attachment to host endo- and epithelial cells, mediate biofilm formation and iron acquisition, and are well-established virulence factors (HOYER et al. 2008; de Groot et al. 2013; Lipke 2018). It has been suggested that expansion of the cell wall protein repertoire, particularly adhesins, is a key step towards the evolution of yeast pathogens (Gabaldón et al. 2016). This is supported by a study showing that several adhesin families independently expanded in *C. glabrata* and close relatives (Gabaldón et al. 2013). Interestingly, studies of pathogenic *Escherichia coli* found that multiple strains independently acquired genes mediating intestinal adhesion, giving precedence to the hypothesis from a different kingdom (Reid et al. 2000).

Despite the importance of adhesins in both the evolution and virulence of *Candida* pathogens, there is a lack of detailed phylogenetic study for their evolutionary history(Hoyer 2001; Linder and Gustafsson 2008; Gabaldón et al. 2013). Even less is known about their sequence divergence and the role of natural selection in their evolution (Xie et al. 2011). In the

newly emerged *Candida auris*, individual adhesins have been characterized but there is little information about their evolutionary relationship with homologs in other *Candida* species and how their sequence diverged (Kean et al. 2018; Singh et al. 2019; Muñoz et al. 2021). In this study we characterized the detail evolutionary history of a yeast adhesin family and used *C. auris* as a focal group to determine how adhesin sequences diverged under various natural selection forces. To choose a candidate adhesin family in *C. auris*, we compared it with the well-studied *C. albicans*, which belongs to the same CUG-Ser1 clade. Of the known adhesins in *C. albicans*, *C. auris* lacks the Hwp family and has only three Als or Als-like proteins compared with eight Als proteins in *C. albicans* (Muñoz et al. 2018). By contrast, *C. auris* has eight genes with a Hyphal_reg_CWP (PF11765) domain found in the Hyr/Iff family in *C. albicans* (Muñoz et al. 2021). This family was one of the most highly enriched in pathogenic *Candida* species relative to the non-pathogenic ones (Butler et al. 2009). Transcriptomic studies identified two *C. auris* Hyr/Iff-like (Hil) genes as being upregulated during biofilm formation and under antifungal treatment (Kean et al. 2018). Interestingly, isolates from the less virulent *C. auris* Clade II lack five of the eight Hil genes (Muñoz et al. 2021). It is currently not known whether the *C. auris HIL* genes encode adhesins, how they relate to the *C. albicans* Hyr/Iff family genes and how their sequences diverged after duplication.

We show that the Hil family independently expanded multiple times, including in *C. auris* and *C. albicans*. Sequence features and predicted structures of the effector domain indicated that most of the yeast Hil family encode adhesins, including all eight members in *C. auris*, Rates of nonsynonymous-to-synonymous substitutions revealed varying strengths of selective constraint and positive selection acting on the effector domain during the family expansion. Rapid divergence in the repeat-rich central domain led to large variations in length and β-aggregation potential between paralogs and among strains of *C. auris*, likely contributing to phenotypic diversity in adhesion and possibly in virulence.

Results

Phylogenetic distribution of the Hyr/Iff-like (Hil) family and its potential to encode adhesin

The Hyr/Iff family was first identified and characterized in *Candida albicans* (Bailey et al. 1996; Richard and Plaine 2007). The family is defined by its N-terminal Hyphally regulated Cell Wall Protein domain (Hyphal_reg_CWP, PF11765), followed by a highly variable central domain rich in tandem repeats (Boisramé et al. 2011). Because the effector domain is more conserved than the repeat region and plays a prominent role in mediating adhesion in known yeast adhesins

98 (Willaert 2018), here we define the Hyr/Iff-like (Hil) family as the group of evolutionarily related
99 proteins sharing the Hyphal_reg_CWP domain, different from a previous definition based on
100 sequence similarity in either the Hyphal_reg_CWP domain or the repeat region (Butler et al. 2009).
101 To determine the phylogenetic distribution of the Hil family and its association with the
102 pathogenic potential of species, we performed BLASTP searches using the Hyphal_reg_CWP
103 domain from three distantly related Hil homologs as queries (from *C. auris*, *C. albicans* and *C.*
104 *glabrata*). We scrutinized the database hits and searched additional assemblies to ensure that
105 their sequences are complete and accurate given the available genome assemblies (Text S1).
106 Using the criteria of *E*-value<10^{-5} and query coverage>50%, we identified a total of 215 proteins
107 containing the Hyphal_reg_CWP domain from 32 species (Fig. 1A, Table S1). No credible hits
108 were identified outside the budding yeast subphylum even after a lower *E*-value cutoff of 10^{-3}
109 was tested, suggesting that this family is specific to this group (Materials and Methods). Species
110 with eight or more Hil family genes fell largely within the Multi-Drug Resistant (MDR) and the
111 Candida/Lodderomyces (CaLo) clades, which include *C. auris* and *C. albicans*, respectively.
112 Only three such species were found outside of the two clades: *C. glabrata*, *M. bicuspidata* and
113 *K. africana*. *C. glabrata* is a major opportunistic pathogen that is more closely related to *S.*
114 *cerevisiae* than to most other *Candida* species (Dujon et al. 2004; Butler et al. 2009; Gabaldón
115 et al. 2013). *M. bicuspidata* is part of the CUG-Ser1 clade. While not a pathogen in humans, it is
116 a parasite of freshwater animals (Hall et al. 2010; Jiang et al. 2022). *K. africana* is not closely
117 related to any known yeast pathogen and its ecology is poorly understood (Gordon et al. 2011).
118 We then asked how many of the Hil family genes in each species are likely to encode
119 yeast adhesins. To get an initial estimate, we combined a Machine Learning tool for predicting
120 fungal adhesins (Chaudhuri et al. 2011) with predictions for the N-terminal signal peptide and C-
121 terminal GPI-anchor sequence, two features shared by the majority of known fungal adhesins
122 (Lipke 2018). Half of all Hil homologs passed all three tests (Fig. 1A). Notably, *M. bicuspidata*
123 has the largest Hil family among all species, but none of its 29 Hil genes passed all tests. We
124 found most of the identified hits in this species were short relative to the rest of the family (Fig.
125 S1), and 10 of the 29 hits were annotated as being incomplete in the RefSeq database. Further
126 analyses with a better assembled genome and functional studies are needed to determine if the
127 Hil family in this species has unique properties and functions.

128 **Independent expansion of the Hil family in multiple pathogenic *Candida* lineages**

129 Pathogenic yeast species have on average a larger Hil family and also more of its members
130 were predicted to encode adhesins than in low pathogenic-potential species (Fig. 1B, t-test with
131 unequal variance and Mann-Whitney U test both yielded $P < 0.005$, one-sided test). This naive

132 comparison doesn't account for phylogenetic relatedness between species and could result in a
133 false positive association (Levy et al. 2017; Bradley et al. 2018). To address this, we performed
134 phylogenetic logistic regression, which uses the known phylogeny to specify the residual
135 correlation structure among species with shared ancestry (Ives and Garland 2010). We tested
136 for associations between the pathogen status with either the total number of Hil homologs or the
137 number of putative adhesins in each species. Both tests were significant (P = 0.005 and 0.007,
138 respectively). Together, these results strongly support an enrichment of the Hil family and the
139 putative adhesins therein among the pathogenic yeast species.

140 Some adhesin families have undergone independent expansions even among closely
141 related species (Gabaldón et al. 2013). This would result in overestimation of the phylogenetic
142 signal in the above analysis. To further characterize the evolutionary history of the Hil family,
143 including among closely related *Candida* lineages, we reconstructed a species tree-aware
144 maximum likelihood phylogeny for the Hil family based on the Hyphal_reg_CWP domain
145 alignment (Fig. 1C, Fig. S2). We found that homologs from the MDR clade and the Candida /
146 Lodderomyces (CaLo) clade separated into two groups, suggesting that the duplications of the
147 Hil family genes in the two clades occurred independently. To better illustrate the history of gene
148 duplications in the Hil family, we reconciled the gene tree with the species tree and mapped the
149 number of duplications onto the species phylogeny (Materials and Methods). The result showed
150 that the Hil family has independently expanded multiple times, not only between clades but also
151 among closely related species within a clade, such as in *C. albicans* and *C. tropicalis* (Fig. 1D).

152 **Sequence features of the *C. auris* Hil family support their adhesin status**

153 Experiments have demonstrated that Hil family members function as adhesin in *C. albicans* and
154 more recently for one member in *C. glabrata* (Bailey et al. 1996; Boisramé et al. 2011; Reithofer
155 et al. 2021; Rosiana et al. 2021). To further evaluate the adhesin function of Hil family proteins,
156 we focused on *C. auris*, in which Hil family members were implicated in biofilm formation and
157 response to antifungal treatments, but still remain poorly characterized (Kean et al. 2018). We
158 named the eight *C. auris* Hil family proteins Hil1-Hil8 ordered by their length (Table S2). This
159 differs from the literature, which referred to them by their most closely related Hyr/Iff genes in *C.*
160 *albicans* (Kean et al. 2018; Jenull et al. 2021; Muñoz et al. 2021). The renaming was to avoid
161 the incorrect implication of one-to-one orthology between the two species (Fig. 1C).

162 To further assess the adhesin potential for the *C. auris* Hil family, we compared their
163 domain architecture and sequence features to those typical of known yeast adhesins, including
164 a signal peptide, an effector domain, a Ser/Thr-rich and highly glycosylated central domain with
165 tandem repeats and β-aggregation prone sequences and a GPI-anchor signal (Fig. 2A) (de

166 Groot et al. 2013; Lipke 2018). All eight *C. auris* Hil proteins followed this domain architecture
167 (Fig. 2B). Hil1-4 were additionally characterized by an array of regularly spaced β-aggregation
168 prone sequences (red ticks below the protein, Fig. 2B). All eight proteins also had elevated
169 Ser/Thr frequencies in their central domain and were predicted to be heavily O-glycosylated
170 (Fig. 2C). Predicted N-glycosylation was rare except in Hil5 and Hil6 (Fig. 2C). The overall
171 Ser/Thr frequencies in the Hil family proteins were significantly elevated compared with the rest
172 of the proteome (Fig. S3). All eight members were predicted to be fungal adhesins by
173 FungalRV, a support vector machine-based classifier that showed high sensitivity and specificity
174 in eight pathogenic fungi based on sequence features (Chaudhuri et al. 2011).

175 **Hyphal_reg_CWP domain in the Hil family is predicted to adopt a β-helical fold similar to**
176 **unrelated bacterial adhesin binding domains**

177 Crystal structures of the effector domain in several yeast adhesin families, including Als, Epa
178 and Flo, revealed carbohydrate or peptide binding activities supporting the proteins' adhesin
179 functions (Willaert 2018). The structure of the Hyphal_reg_CWP domain in the Hil family in this
180 study has not yet been experimentally determined. However, crystal structures for the effector
181 domains of two Adhesin-like Wall Proteins (Awp1 and Awp3b) in *C. glabrata*, which are distantly
182 related to those in the Hil family, were recently reported, and the predicted structure of one of *C.*
183 *glabrata*'s Hil family members (Awp2) was found to be highly similar to the two solved structures
184 (Reithofer et al. 2021). We used AlphaFold2 (Jumper et al. 2021) to predict the structures of the
185 effector domain for two *C. auris* Hil proteins, Hil1 and Hil7 (Fig. 3A, B). Both resemble the *C.*
186 *glabrata* Awp1 effector domain (Fig. 3C), consisting of a right-handed β-helix at the N-terminus
187 followed by an α-crystallin fold. There are three β-strands in each of the 9 rungs in the β-helix,
188 stacked into three parallel β-sheets (Fig. 3D). The α-crystallin domain consists of seven β-
189 strands forming two antiparallel β-sheets, adopting an immunoglobulin-like β-sandwich fold (Fig.
190 3E) (Koteiche and Mchaourab 1999; Stamler et al. 2005).

191 The β-strand-rich structure is typical of effector domains in known yeast adhesins, but
192 the β-helix fold at the N-terminus is uncommon (Willaert 2018). Proteins with a β-helix domain
193 often have carbohydrate-binding capabilities and act as enzymes, e.g., hydrolase and pectate
194 lyase (SCOP ID: 3001746). To gain further insight into Hyphal_reg_CWP domain's function, we
195 searched the PDB50 database for structures similar to what was predicted for *C. auris* Hil1
196 using DALI (Holm 2022). We identified a number of bacterial adhesins with a highly similar β-
197 helix fold but no α-crystallin domain (Table S3), e.g., Hmw1 from *H. influenzae* (PDB: 2ODL),
198 Tāpirins from *C. hydrothermalis* (PDB: 6N2C), TibA from enterotoxigenic *E. coli* (PDB: 4Q1Q)
199 and SRRP from *L. reuteri* (PDB: 5NY0). For comparison, the binding region of the Serine Rich

200 Repeat Protein 100-23 ($SRRP_{100-23}$) from *L. reuteri* was shown in Fig. 3F (Sequeira et al. 2018).
201 Together, these results strongly suggest that the Hyphal_reg_CWP domain in the *C. auris* Hil
202 family genes mediates adhesion. Additionally, the low sequence identity (12-15%) between the
203 yeast Hyphal_reg_CWP domain and the bacterial adhesins' binding regions further suggests
204 the two groups have convergently evolved a similar structure to achieve adhesion functions.

205 **Rapid divergence of the repeat-rich central domain in Hil family proteins in *C. auris***

206 While the overall domain architecture is well conserved, the eight Hil family proteins in *C. auris*
207 differ significantly in length and sequence of their central domains (Fig. 2B). While not involved
208 in ligand binding, central domains in yeast adhesins are known to play a critical role in mediating
209 adhesion: the length and stiffness of the central domain are essential for elevating and exposing
210 the effector domain (Frieman et al. 2002; Boisramé et al. 2011); and the tandem repeats and β-
211 aggregation sequences within them directly contribute to adhesion by mediating homophilic
212 binding and amyloid formation (Rauceo et al. 2006; Otoo et al. 2008; Frank et al. 2010; Wilkins
213 et al. 2018). Thus, divergence in the central domain of the Hil family has the potential to lead to
214 phenotypic diversity, as shown in *S. cerevisiae* (Verstrepen et al. 2004; Verstrepen et al. 2005).
215 To determine how the central domain sequences evolved in the *C. auris* Hil family, we
216 used dot plots both to reveal the tandem repeat structure within each protein and to examine the
217 similarity among the paralogs. We found that *C. auris* Hil1 to Hil4 share a ~44 aa repeat unit,
218 whose copy number varies between 15 and 46, driving their differences in protein length (Fig.
219 4A). These repeats have conserved periods and sequences (Fig. 4B, Fig. S4). There are two
220 interesting features of this 44 aa repeat unit: a) it contains a heptapeptide "GVVIVTT" that is
221 predicted to be strongly β-aggregation prone, which explains the large number of regularly
222 spaced β-aggregation motifs in Hil1-Hil4 (Fig. 2B); b) it is predicted to form three β-strands in
223 the same orientation (Fig. 4B), raising an interesting question of whether the tandem repeats
224 may adopt a β-structure similar to that of the effector domain. Hil7 and Hil8 encode the same
225 repeat unit but have only one copy (Fig. 4A, red boxes). By contrast, Hil5 and Hil6 encode very
226 different low complexity repeats with a period of ~5 aa and between 15 to 49 copies (Fig. 4C, D)
227 with relatively low Ser/Thr frequencies (Fig. 2C). Another consequence of encoding only one or
228 zero copy of the 44 aa repeat unit found in Hil1-Hil4 is that Hil5-Hil8 are predicted to have 2-4 β-
229 aggregation prone sequences in contrast to 21-50 in Hil1-Hil4. For comparison, characterized
230 yeast adhesins contain 1-3 such sequences at a cutoff of >30% β-aggregation potential
231 predicted by TANGO (Fernandez-Escamilla et al. 2004; Ramsook et al. 2010; Lipke 2018). The
232 variable lengths, Ser/Thr frequencies and distribution of β-aggregation sequences suggest that

233 the 8 different Hil proteins in *C. auris* are non-redundant, likely playing distinct roles in cell
234 adhesion and other cell-wall related phenotypes.
235 Because tandem repeats are prone to recombination-mediated expansions and
236 contractions, we asked if there are variable numbers of tandem repeats (VNTR) among strains
237 in *C. auris*, which could generate diversity in cell adhesive properties as shown in *S. cerevisiae*
238 (Verstrepen et al. 2005). To answer this question, we identified homologs of Hil1-Hil4 in nine *C.*
239 *auris* strains from three geographically-stratified clades (Muñoz et al. 2018; Muñoz et al. 2021).
240 The genomes of these strains were *de novo* assembled using long-read technologies (Table
241 S4), which allowed us to confidently assess copy number variations within tandem repeats. We
242 identified a total of eight indel polymorphisms in Hil1-Hil4 (Table S5, example alignments in Fig.
243 S5). Except for one 16 aa deletion that is in a single Clade III strain, all seven other indels span
244 one or multiples of the repeat unit and affect all strains within a clade. This is consistent with
245 them being driven by recombination between repeats. The agreement within clades additionally
246 show the indels are not due to sequencing / assembly artifacts, which are not expected to follow
247 the clade labels. As previously reported, Clade II strains lack five of the eight Hil family proteins,
248 including Hil1-4 (Muñoz et al. 2021). Our phylogenetic analysis further showed that this was due
249 to gene losses within Clade II (Fig. S6). The potential relationship between the Hil family size
250 and the virulence profiles of Clade II strains is discussed later.

251 **Natural selection on the effector domain during the Hil family expansion in *C. auris***

252 Gene duplication provides raw materials for natural selection and is often followed by a period of
253 relaxed functional constraints on one or both copies, allowing for sub- or neo-functionalization
254 (Zhang 2003; Innan and Kondrashov 2010). Positive selection can be involved in the process,
255 which can lead to a ratio of nonsynonymous to synonymous substitution rates dN/dS > 1 (Yang
256 1998). Here we ask if the Hyphal_reg_CWP domain in *C. auris* Hil1-Hil8 experienced relaxed
257 selective constraints and/or positive selection following gene duplications, the latter of which
258 would suggest functional diversification. We chose to focus on the Hyphal_reg_CWP domain
259 because of its functional importance and because the high-quality alignment in this domain
260 allowed us to make confident evolutionary inferences (Fig. S7).
261 Because gene conversion between paralogs can cause distinct genealogical histories for
262 different parts of the alignment and mislead evolutionary inferences (Casola and Hahn 2009),
263 we first identified putatively non-recombining partitions using GARD (Kosakovsky Pond et al.
264 2006) (Fig. S8), and chose two partitions, P1-414 and P697-981, for maximum-likelihood based
265 analyses using PAML (Yang 2007) (Fig. 5A).

266 We first tested if a subset of the sites evolved under positive selection consistently on *all*
267 branches. We found moderate evidence supporting the hypothesis for the P697-981 partition,
268 where the M8 vs. M7 and M8 vs. M8a tests were significant at a 0.01 level, but the conservative
269 test M2a vs M1a was not (Table S6). All three tests were insignificant for the P1-414 partition.
270 Next, we tested for elevated dN/dS on selected branches of the tree, sign of relaxed selective
271 constraints or positive selection. We first estimated the dN/dS for each branch using a free-ratio
272 model and designated those with dN/dS greater than 10 as the "foreground" (Fig. 5B, C, "FG").
273 We found strong evidence for the FG branches to have a higher dN/dS than the remainder of
274 the tree (log-likelihood ratio test $P < 0.01$, Fig. 5D). There is no evidence, however, for the
275 dN/dS across the entire domain on the FG branches to be greater than 1 (Fig. 5D, *a*, row 2). We
276 then tested the more realistic scenario, where a subset of the sites on the FG branches were
277 subject to positive selection. Using the branch-site test 2 as defined in (Zhang et al. 2005), we
278 found evidence for positive selection on a subset of the sites on the FG branches for both
279 partitions (log-likelihood ratio test $P < 0.01$), and identified residues in both as candidate targets
280 of positive selection with a posterior probability greater than 0.99 (Fig. 5D). We conclude that
281 there is strong evidence for relaxed selective constrain on the Hyphal_reg_CWP domain on
282 some branches following gene duplications; there is also evidence for positive selection acting
283 on a subset of the sites on those branches. However, as the free-ratio model estimates were
284 noisy and the empirical bayes method used to identify the residues under selection lacks power
285 (Zhang et al. 2005) and can produce false positives (Nozawa et al. 2009), the specific branches
286 and residues implicated must be interpreted with caution.

287 **The yeast Hil family has adhesin-like domain architecture with rapidly diverging central**
288 **domain sequences**

289 We next examined the entire yeast Hil family to reveal the broader patterns of their evolution.
290 We found that the Hil family in general has elevated Ser/Thr content compared with the rest of
291 the proteome (Fig. S9). Moreover, the majority encode tandem repeats in the central domain
292 (Fig. 6A) and contain predicted β-aggregation prone sequences (Fig. 6B). Together, these
293 features further suggest that a large fraction of the yeast Hil family members likely encode
294 fungal adhesins. While these key features typical of yeast adhesins are conserved, the yeast Hil
295 family exhibits extreme variation in protein length, tandem-repeat content as well as in β-
296 aggregation potential (Fig. 6A, B, S10), extending the pattern seen in *C. auris* (Fig. 2). The
297 length of the protein outside of the Hyphal_reg_CWP domain has a mean ± standard deviation
298 of 822.4±785.8 aa and a median of 608.5 aa. This large variation in protein length is almost
299 entirely driven by the tandem repeats (Fig. 6C, linear regression slope = 1.0, $r^2 = 0.83$). A subset

300 of the Hil proteins (vertical bar in Fig. 6A, B) stand out in that 1) they are longer than the rest of
301 the family (1745 vs 770 aa, median protein length) and 2) they have an unusually large number
302 of β-aggregation prone motifs (25 vs 6, median number of TANGO hits per protein). The motifs
303 in this group of proteins are regularly spaced as a result of being part of the tandem repeat unit
304 (median absolute deviation, or MAD, of distances between adjacent TANGO hits less than 5 aa,
305 Fig. 6D). The motif "GVVIVTT" and its variants account for 61% of all hits in this subset and are
306 not found in significant number in the rest of the family. Together, these observations combined
307 with previous experimental studies showing a direct impact of adhesin length and β-aggregation
308 potential on their functions (Verstrepen et al. 2005; Lipke et al. 2012) lead us to propose that the
309 rapid divergence of the Hil family following the parallel expansion led to functional diversification
310 in adhesion in pathogenic yeasts and may have contributed to their enhanced virulence.

311 **The yeast Hil family genes are preferentially located near chromosome ends**

312 Several well-characterized yeast adhesin families, including the Flo family in *S. cerevisiae* and
313 the Epa family in *C. glabrata*, are enriched in the subtelomeres (Teunissen and Steensma 1995;
314 De Las Peñas et al. 2003; Xu et al. 2020; Xu et al. 2021). This region is associated with high
315 rates of SNPs, indels and copy number variations, and can undergo ectopic recombination that
316 enables the spread of genes between chromosome ends or their losses (Mefford and Trask
317 2002; Anderson et al. 2015). To determine if the Hil family is also enriched in the subtelomeric
318 region, we compared their chromosomal locations with the background gene density distribution
319 (Fig. 7A) in species with a chromosomal level assembly (Table S7). To account for the shared
320 evolutionary history, we selected one species per closely related group such that the Hil family
321 homologs in these species were mostly derived through independent duplications based on our
322 gene tree (Fig. S2). The result showed that the Hil family genes are indeed enriched at
323 chromosomal ends (Fig. 7B). A goodness-of-fit test confirmed that the difference between the
324 chromosomal locations of the Hil family and the genome background is highly significant (P =
325 1.3×10^{-12}). As ectopic recombination between subtelomeres has been suggested to underlie the
326 spread of gene families (Anderson et al. 2015), we hypothesize that the enrichment of the Hil
327 family towards the chromosome ends is both a cause and consequence of its parallel expansion
328 in different *Candida* lineages.

329 **Discussion**

330 The repeated emergence of yeast human pathogens in the Saccharomycetes class poses
331 serious health threats, as many emerging pathogenic species are multi-drug resistant or quickly
332 gain resistance (Lamoth et al. 2018; Srivastava et al. 2018). This raises an evolutionary

333 question: are there shared genomic changes in independently derived *Candida* pathogens,
334 which could be key factors behind host adaptation? Yeast adhesin families were among the
335 most enriched gene families in pathogenic lineages relative to the low pathogenic potential
336 relatives (Butler et al. 2009). It has been proposed that expansion of adhesin families could be a
337 key step in the emergence of novel yeast pathogens (Gabaldón et al. 2016). However, detailed
338 phylogenetic studies supporting this hypothesis are rare (Gabaldón et al. 2013), and far less is
339 known about how their sequences diverge and what selective forces are involved during the
340 expansions (Xie et al. 2011; Muñoz et al. 2021). In this study, we found that the Hyr/Iff-like (Hil)
341 family, defined by the conserved Hyphal_reg_CWP domain, is significantly enriched among
342 distantly related pathogenic clades (Fig. 1A, B). This resulted from independent expansion of
343 the family in these clades, including among closely related species (Fig. 1C, D). We also
344 showed that the protein sequences diverged extremely rapidly after duplications, driven mostly
345 by the evolution of the tandem repeats and resulting in large variations in protein length, Ser/Thr
346 content and β-aggregation potential (Fig. 2B, C, Fig. 6). Our evolutionary analyses revealed
347 evidence of relaxed selective constraint and a potential role of positive selection acting on the
348 Hyphal_reg_CWP domain during the family's expansion in *C. auris* (Fig. 5). We also found the
349 Hil family to be strongly enriched near chromosomal ends (Fig. 7). Overall, our results support
350 the hypothesis that expansion and diversification of adhesin families is a key step towards the
351 emergence of yeast pathogens.

352 **Genome assembly quality limits gene family evolution studies**

353 Like any study of multi-gene family evolution, our work relies on and is limited by the quality of
354 the genome assemblies. Two additional challenges in our study are due to the fact that Hil
355 family genes are rich in tandem repeats (Fig. 2B, 6A), and many are located near chromosome
356 ends (Fig. 7B), both of which pose problems for genome assemblies. For example, we found
357 significant disagreement in length for 8 of the 16 Hil proteins in *C. tropicalis* between a long-read
358 assembly and the RefSeq assembly, consistent with a recent study (Oh et al. 2020) (Table S8);
359 in *C. glabrata*, we identified 13 Hil family genes in a long-read assembly (GCA_010111755.1) vs
360 3 in the RefSeq assembly (GCF_000002545.3); 12 of the 13 genes were in the subtelomeres
361 (Xu et al. 2020). However, similar analyses in additional species didn't reveal these problems,
362 suggesting that the issues were at least in part due to difficulties in some genomes (Text S1).
363 Nonetheless, we acknowledge the possibility of missing homologs and inaccurate sequences,
364 especially in the tandem-repeat region. We thus believe the expected improvements in genome
365 assemblies due to advances in long-read sequencing technologies will be crucial for future
366 studies of the adhesin gene family in yeasts. It is worth noting that our main conclusions about

367 the parallel expansion of the Hil family and its rapid divergence patterns are robust with respect
368 to isolated problems as described above. Also, the long-read technology-based and *de novo*
369 assembled genomes for *C. auris* strains allowed us to confidently assess variation in the Hil
370 family size and tandem repeat copy number between paralogs and among individual strains
371 (Table S4). The accuracy of the tandem-repeat sequences in multiple strains in this species is
372 supported by the conservation of repeat copy numbers within clades (Table S5).

373 **Evidence for adhesin functions in the Hil family**

374 A few members of the Hil family, e.g., Iff4 in *C. albicans* and Awp2 in *C. glabrata* were shown to
375 mediate adhesiveness to polystyrene (Fu et al. 2008; Kempf et al. 2009; Reithofer et al. 2021).
376 While further experimental studies are needed to establish the adhesin functions of other Hil
377 family members, our work provided bioinformatic support for a large fraction of the Hil family as
378 encoding adhesins (Fig. 2, 6). The predicted β-helix fold of the Hyphal_reg_CWP domain (Fig.
379 3), while unusual among characterized yeast adhesins (Willaert 2018), is found in many
380 virulence factors residing on the surface of bacteria or viruses as well as enzymes that degrade
381 or modify polysaccharides (Table S3) (Kajava and Steven 2006). The elongated shape and rigid
382 structure of the β-helix are consistent with the functional requirements of adhesins, including the
383 need to protrude from the cell surface and the capacity for multiple binding sites along its length
384 that facilitate adhesion. In a bacterial adhesin – the serine rich repeat protein (SRRP) from the
385 Gram-positive bacterium, *L. reuteri* – a protruding, flexible loop in the β-helix was proposed to
386 serve as a binding pocket for its ligand (Sequeira et al. 2018). Such a feature is not apparent in
387 the predicted structure of the Hyphal_reg_CWP domain. Further studies are needed to elucidate
388 the mechanism of action of this domain and its potential substrates.

389 The cross-kingdom similarity in adhesin effector domain structure is intriguing in several
390 ways. First, it suggests convergent evolution in bacteria and yeasts. Second, it suggests that
391 what is known about the structure-function relationship in bacteria can provide insight into the
392 Hyphal_reg_CWP domain in yeast. Notably, the *Lr*SRRP shows a pH-dependent substrate
393 specificity that is potentially adapted to distinct host niches (Sequeira et al. 2018). Finally, the
394 similar structure and function of the bacterial and yeast adhesins could mediate cross-kingdom
395 interactions in natural and host environments (Uppuluri et al. 2018).

396 However, not all Hil family homologs are likely to encode adhesins. Sequence features
397 suggest some Hil family proteins may have non-adhesin functions. For example, 39 of 193 Hil
398 proteins (homologs labeled as incomplete were excluded) have the requisite signal sequence,
399 but lack a GPI anchor attachment site (Fig. S1). One of them, Iff11 in *C. albicans*, was shown to
400 be secreted, and a null mutant of it was found to be hypersensitive to cell wall-damaging agents

401 and less virulent in a murine systemic infection model (Bates et al. 2007). Moreover, 75% of
402 these “SP+, gpi-“ proteins are shorter than 600 amino acids, in contrast to only 4% of the 117
403 proteins having both a signal peptide and a GPI anchor attachment site. Such short, secreted
404 proteins with tandem repeat sequences identical or similar to those present in the cell-wall
405 associated Hil protein counterparts may serve an important regulatory function by bundling with
406 wall associated adhesins as previously suggested for similar subclass of proteins within the Als
407 family (Oh et al. 2019). It is possible that the Hil family has evolved diverse functions broadly
408 related to cell adhesion.

409 **Ongoing diversification of the Hil family within species**

410 In addition to the parallel expansion and the subsequent rapid sequence divergence in the Hil
411 family between species, we and others also revealed population level variation in both the family
412 size and sequences within *C. auris* (Fig. S5, S6, Table S5) (Muñoz et al. 2021). Notably, among
413 the four geographically stratified clades, Clade II strains lost five of the eight Hil family members
414 (Fig. S6). Besides missing members of the Hil family, Clade II strains also lack seven of the
415 eight members of another GPI-anchor family that is specific to *C. auris* (Muñoz et al. 2021).
416 These coincide with the finding that Clade II strains were mostly associated with ear infections
417 (57/61 isolates according to (Kwon et al. 2019)) rather than hospital outbreaks, as reported for
418 strains from the other clades, and that they were generally less resistant to antifungal drugs
419 (Kwon et al. 2019; Welsh et al. 2019). This raises the question of whether the smaller adhesin
420 repertoire in Clade II strains limits their adhesive capability and results in a different pathology.
421 Similar expansion and contraction of adhesin families have been shown for the *C. glabrata* Hil
422 family (AWP Cluster V) and Epa family (Marcet-Houben et al. 2022), suggesting that dynamic
423 evolution of adhesin families in pathogenic yeasts could be a common pattern. Variations in the
424 tandem repeat copy number in Hil1-Hil4 among *C. auris* strains is also intriguing (Fig. S5). Prior
425 studies of the *S. cerevisiae* Flo proteins have shown that protein lengths directly impact cells’
426 adhesion phenotypes (Verstrepen et al. 2005) and thus population level variation in adhesin
427 length could further contribute to phenotypic diversity. Lastly, scans for selective sweep in *C.*
428 *auris* identified Hil and Als family members as being among the top 5% of all genes, suggesting
429 that adhesins are targets of natural selection in the recent evolutionary history of this newly
430 emerged pathogen (Muñoz et al. 2021).

431 Diversification of adhesin repertoire within a strain can arise from a variety of molecular
432 mechanisms. For example, chimeric proteins generated through recombination between Als
433 family members or between an Als protein’s N terminal effector domain and an Hyr/Iff protein’s
434 repeat region have been shown (Butler et al. 2009; Zhao et al. 2011; Oh et al. 2019). Some of

435 the adhesins with highly diverged central domains may have arisen in this manner (Fig. S10).
436 Gene conversion between members of the same family can also drive the evolution of adhesin
437 families within a species, as shown in *S. cerevisiae* and *C. glabrata* (Verstrepen et al. 2004;
438 Marcet-Houben et al. 2022). Evidence of this in the Hil family was revealed in our analysis of
439 recombination within the effector domain in *C. auris* (Fig. S8).

440 **Special properties of the central domain in *C. auris* Hil1-Hil4 and related Hil proteins**

441 A subset of Hil proteins represented by *C. auris* Hil1-Hil4 (Fig. 6A, B, vertical bar) stand out in
442 that they are much longer on average and encode a large number of β-aggregation prone
443 sequences compared with the rest of the family (Fig. 6B, D). Behind these properties is a
444 conserved ~44 aa repeat unit containing a highly β-aggregation prone sequence ("GVVIVTT"
445 and its variants) (Fig. 4B). β-aggregation prone sequences and the amyloid-like interaction they
446 mediate have been extensively studied, especially in the Als protein family in *C. albicans*: they
447 were experimentally shown to mediate aggregation (Otoo et al. 2008; Ramsook et al. 2010) and
448 were crucial for forming protein clusters on cell surfaces known as nanodomains in response to
449 physical tension or sheer forces (Alsteens et al. 2010; Lipke et al. 2012). Recently, they were
450 also shown to mediate cell-cell *trans* interactions via homotypic protein binding (Dehullu et al.
451 2019; Ho et al. 2019). This may underlie biofilm formation and kin discrimination (Smukalla et al.
452 2008; Brückner et al. 2020; Lipke et al. 2021). Most known yeast adhesins, including the Als
453 family proteins, encode one to three β-aggregation prone sequences (Ramsook et al. 2010).
454 Unusually, *C. auris* Hil1-Hil4 and their close relatives is that they have as many as 50 such
455 sequences, with each predicted by TANGO to have ~90% probability of aggregation, whereas
456 the positive threshold for the algorithm is only >5% over 5-6 residues (Fernandez-Escamilla et
457 al. 2004). The structural implications of the vast number of β-aggregation prone motifs may be
458 that such tandem repeat domains are constitutively amyloid in nature, rather than requiring force
459 or other stimuli as in the Als proteins. The functional implications are unclear without the
460 requisite experimental tests. However, we speculate that variations in protein length and β-
461 aggregation potential resulting from the central domain divergence could directly impact the
462 adhesion functions as previously suggested (Verstrepen et al. 2005; Boisramé et al. 2011; Lipke
463 et al. 2012).

464 **Structural predictions of the tandem repeat region in *C. auris* Hil1 and Hil2**

465 Given the larger number of ~44 aa repeats in the central domain of *C. auris* Hil1-Hil4 and the
466 prediction that each repeat encodes 3-4 short consecutive β-strands (Fig 4B), we wondered
467 what structural properties this region may have and how it could contribute to the adhesion

468 function. We explored this question using threading based structural prediction tools such as I-
469 TASSER (Yang et al. 2015) and pDOMThreader (Lobley et al. 2009). For the tandem repeat
470 region in the central domain of Hil1, I-TASSER identified (S)-layer protein (SLP) structures (e.g.,
471 RsaA from *C. crescentus*, SbsA and SbsC from *G. sterotherophilus*) as among the top structural
472 analogs. These β-strand-rich structures are known to self-assemble to form a 2-dimentional
473 array on the surface of bacteria, mediating a range of functions including adhesion to host cells
474 in pathogens (Fagan and Fairweather 2014). pDOMThreader analyses of the central domains in
475 Hil1 and Hil2 identified a different set of templates, namely bacterial self-associating proteins
476 including Ag43a from uropathogenic *E. coli*, pertactin from *B. pertussis* and the *H. influenzae*
477 hap adhesin. Interestingly, they have β-helical structures like the Hyphal_reg_CWP domain, and
478 the β-helices in them were involved in cell-cell interaction via an interface along the long
479 solenoidal axis for homotypic interactions, which mediate bacterial clumping (Heras et al. 2014)
480 and lead to biofilm formation in *H. influenzae* (Meng et al. 2011). We speculate that the long
481 repeat regions in Hil1 and Hil2 may similarly mediate cell-cell interactions in *C. auris*.
482 The possibility of the central domains in Hil1 and Hil2 forming a β-helix is interesting in
483 that β-helix is one of the commonly described structural motifs in functional amyloids, e.g., HET-
484 s from the fungus *Podospora anserina* (Wasmer et al. 2008). Such a solenoid-type amyloid is
485 distinguished from other amyloid types in that the β-sheets formed by repeats within the same
486 protein, rather than among distinct monomeric proteins, are suggested to be stabilized not only
487 by polar zippers and hydrophobic contacts, but also by electrostatic interactions between the
488 alternating β-strands (Willbold et al. 2021). Other examples of amyloid forming proteins with a
489 predicted β-helix structure include the imperfect repeat domain in the human premelanosome
490 protein Pmel17 (Louros et al. 2016) and the extracellular curli proteins of Enterobacteriaceae
491 that are involved in biofilm formation and adhesion to host cells (Shewmaker et al. 2009). The
492 proposed solenoidal structure of the central domain of Hil1-Hil4 like proteins, if true, would have
493 two significant implications. First, it confers the necessary rigidity and extended conformation
494 required for cell wall anchored adhesins to extend into the surrounding extracellular milieu.
495 Second, the numerous β-strand rich repeats each containing a highly amyloid prone heptameric
496 sequence, and capable of wrapping into a solenoidal shaped stack, is likely to substantially
497 reduce the rate-limiting nucleation step, which limits the formation of, e.g., an Aβ amyloid fiber.
498 This would allow the formation of extracellular extensions at low protein concentrations without
499 the need for an extensive fiber lengthening process via the incorporation of additional
500 monomeric units. Finally, the observation of solenoid-mediated intercellular interactions in the
501 Hap adhesins suggests that Hil proteins may likewise have a biofilm related function.

502 **Genomic context**

503 As reported by (Muñoz et al. 2021), we found that the Hil family genes are preferentially located
504 near chromosomal ends in *C. auris* and also in other species examined (Fig. 7). This is similar
505 to previous findings for the Flo and Epa families (Teunissen and Steensma 1995; De Las Peñas
506 et al. 2003; Xu et al. 2020; Xu et al. 2021), as well as the Als genes in some species (Oh et al.
507 2021). This location bias of the Hil and other adhesin families is likely a key mechanism for their
508 dynamic expansion and sequence evolution via ectopic recombination (Anderson et al. 2015)
509 and by Break-Induced Replication (Bosco and Haber 1998; Sakofsky and Malkova 2017; Xu et
510 al. 2021). Another potential consequence of the Hil family genes being located in subtelomeres
511 is that they may be subject to epigenetic silencing as an additional regulatory mechanism, which
512 can be derepressed in response to stress (Ai et al. 2002). Such epigenetic regulation of the
513 adhesin genes was found to generate cell surface heterogeneity in *S. cerevisiae* (Halme et al.
514 2004) and lead to hyperadherent phenotypes in *C. glabrata* (Castaño et al. 2005).

515 **Concluding remarks**

516 To address the lack of candidate adhesins in *C. auris*, we identified and characterized the
517 Hyr/Iff-like (Hil) family in this species and all yeasts. Based on our results, we hypothesize that
518 expansion and diversification of adhesin gene families is a key step towards the evolution of
519 fungal pathogenesis and that variation in the adhesin repertoire contributes to within and
520 between species differences in the adhesive and virulence properties. Future experimental tests
521 of these hypotheses will be important biologically for improving our understanding of the fungal
522 adhesin repertoire, biotechnologically for inspiring additional nanomaterials, and biomedically for
523 advancing the development of *C. auris*-directed therapeutics.
524

525 ## Materials and Methods

526 **RESOURCE AVAILABILITY**

527 **Lead contact**

528 Further information and requests for resources and reagents should be directed to and will be
529 fulfilled by the Lead Contact, Bin Z. He (bin-he@uiowa.edu).

530 **Data and code availability**

531 All raw data and code for generating the intermediate and final results are available at the
532 GitHub repository at https://github.com/binhe-lab/C037-Cand-auris-adhesin. Upon publication,

533 this repository will be digitally archived with Zenodo and a DOI will be minted and provided to
534 ensure reproducibility.

535 **Software and algorithms list**

NAME	REFERENCE	WEB OR DOWNLOAD URL
AlphaFold2	(Jumper et al. 2021)	https://github.com/sokrypton/ColabFold (links to DeepMind Google Colab Notebook)
BLAST+ v2.12.0	(Camacho et al. 2009)	https://blast.ncbi.nlm.nih.gov/
ClipKit	(Steenwyk et al. 2020)	https://github.com/JLSteenwyk/ClipKIT
Clustal Omega v1.2.4	(Sievers et al. 2011)	http://www.clustal.org/omega/
Custom R, Python and shell scripts	This study	https://github.com/binhe-lab/C037-Cand-auris-adhesin
DALI	(Holm 2022)	http://ekhidna2.biocenter.helsinki.fi/dali/
EMBOSS v6.6.0.0	(Rice et al. 2000)	http://emboss.open-bio.org/
FungalRV	(Chaudhuri et al. 2011)	http://fungalrv.igib.res.in/
GeneRax v2.0.1	(Morel et al. 2020)	https://github.com/BenoitMorel/GeneRax
HmmerWeb (hmmscan)	(Potter et al. 2018)	https://www.ebi.ac.uk/Tools/hmmer/search/hmmscan
Jalview v2.11	(Waterhouse et al. 2009)	https://www.jalview.org/
JDotter	(Brodie et al. 2004)	https://4virology.net/virology-ca-tools/jdotter/
NetNGlyc v1.0	(Gupta and Brunak 2002)	https://services.healthtech.dtu.dk/service.php?NetNGlyc-1.0
NetOGlyc v4.0	(Steentoft et al. 2013)	https://services.healthtech.dtu.dk/service.php?NetOGlyc-4.0
PAL2NAL.pl	(Suyama et al. 2006)	http://www.bork.embl.de/pal2nal/
PAML v4.9e	(Yang 2007)	http://abacus.gene.ucl.ac.uk/software/paml.html
PredGPI	(Pierleoni et al. 2008)	http://gpcr.biocomp.unibo.it/pr

NAME	REFERENCE	WEB OR DOWNLOAD URL
		edgpi/
PSIPred	(Buchan and Jones 2019)	http://bioinf.cs.ucl.ac.uk/psipred/
PyMol v2.5.2	(Schrödinger, LLC 2021)	https://pymol.org/
R package - ggtree v3.2.1	(Yu 2020)	https://github.com/YuLab-SMU/ggtree
R package - phylolm	(Ho and Ané 2014)	https://cran.r-project.org/web/packages/phylolm/index.html
R package - rentrez v1.2.3	(Winter 2017)	https://github.com/ropensci/rentrez
R package - treeio v1.18.1	(Wang et al. 2020)	https://github.com/YuLab-SMU/treeio
R v4.1.0	(R Core Team)	https://cran.r-project.org/
RAxML v8.0.0	(Stamatakis 2014)	https://cme.h-its.org/exelixis/web/software/raxml/
RAxML-NG v1.1.0	(Kozlov et al. 2019)	https://github.com/amkozlov/raxml-ng
RStudio v1.4	(RStudio Team 2021)	https://www.rstudio.com/
SignalP 6.0	(Teufel et al. 2022)	http://www.cbs.dtu.dk/services/SignalP/
TANGO v2.3.1	(Fernandez-Escamilla et al. 2004)	http://tango.crg.es/
XSTREAM	(Newman and Cooper 2007)	https://amnewmanlab.stanford.edu/xstream/download.jsp

METHOD DETAILS

Identify Hyr/Iff-like (Hil) family homologs in yeasts and beyond

To identify the Hil family proteins in yeasts and beyond, we used the Hyphal_reg_CWP domain sequence from three distantly related Hil homologs as queries, namely, *C. albicans* Hyr1 (XP_722183.2), *C. auris* Hil1 (XP_028889033) and *C. glabrata* CAGL0E06600g (XP_722183.2).

542 We performed BLASTP searches in the RefSeq protein database with an *E*-value cutoff of $1x10^{-}$
543 ^{5}, a minimum query coverage of 50% and with the low complexity filter on. All hits were from
544 Ascomycota (yeasts) and all but one were from the Saccharomycetes class (budding yeast). A
545 single hit was found in the fission yeast *Schizosacchromyces cryophilus*. Using that hit as the
546 query, we searched all fission yeasts in the nr protein database, with a relaxed E-value cutoff of
547 10^{-3} and identified no additional hits. We thus excluded that one hit from downstream analyses.
548 To supplement the RefSeq database, which lacks some yeast species such as those in the
549 Nakaseomyces genus, we searched the Genome Resources for Yeast Chromosomes (GRYC,
550 http://gryc.inra.fr/). Using the same criteria, we recovered 16 additional sequences. To allow for
551 gene tree and species tree reconciliation, we excluded three species that are not part of the 322
552 species yeast phylogeny (Shen et al. 2018) and not a member of the Multidrug-Resistant clade
553 (Muñoz et al. 2018). Further details, including additional quality control steps taken to ensure
554 that the homolog sequences are accurate and complete, can be found in Text S1. In total, we
555 curated a list of 215 Hil family homologs from 32 species.

556 **Gene family enrichment analysis**

557 To determine if the Hil family is enriched in the pathogenic yeasts, we performed two analyses.
558 In the first analysis, we divided the species into pathogens vs low-pathogenic potential groups
559 and performed a t-test with unequal variance (also known as Welch's test) as well as a non-
560 parametric Mann-Whitney U test to compare the Hil family size in the two groups. For both tests,
561 we used either the total size of the family, or the number of putative adhesins as the random
562 variable, and the results were consistent. We excluded homologs from *M. bicuspidata* because
563 10 of its 29 Hil family proteins were annotated as incomplete in the RefSeq protein database,
564 and also because as a parasite of freshwater crustaceans, it does not fit into either the human
565 pathogen or the low-pathogenic potential group. *S. cerevisiae* was included in the comparison
566 as an example of species with zero members of the Hil family. We chose *S. cerevisiae* because
567 we could be confident about its lack of a Hil family homolog thanks to its well assembled and
568 well annotated genome.

569 In the second test, we used phylogenetic logistic regression (Ives and Garland 2010) to
570 account for the phylogenetic relatedness between species. We used the `phyloglm` function in
571 the `phylolm` package in R, with {method = "logistic_IG10", btol = 50, boot = 100}. The species
572 tree, including the topology and branch lengths, were based on the 322 species phylogeny from
573 (Shen et al. 2018), supplemented by the phylogenetic relationship for the MDR clade based on
574 (Muñoz et al. 2018). The *P*-values based on phylogenetically specified residual correlations
575 were reported.

576 **Phylogenetic analysis of the Hil family and inference of gene duplications and losses**

577 To infer the evolutionary history of the Hil family, we reconstructed a maximum-likelihood tree
578 based on the alignment of the Hyphal_reg_CWP domain. First, we used hmmscan (HmmerWeb
579 version 2.41.2) to identify the location of the Hyphal_reg_CWP domain in each Hil homolog. We
580 used the "envelope boundaries" to define the domain in each sequence, and then aligned their
581 amino acid sequences using Clustal Omega with the parameter {--iter=5}. We then trimmed the
582 alignment using ClipKit with its default smart-gap trimming mode (Steenwyk et al. 2020).
583 RAxML-NG v1.1.0 was run in the MPI mode with the following parameters on the alignment:
584 "raxml-ng-mpi --all --msa INPUT --model LG+G --seed 123 --bs-trees autoMRE". The resulting
585 tree was corrected using GeneRax, which seeks to maximize the joint likelihood of observing
586 the alignment given the gene family tree (GFT) and observing the GFT given the species
587 phylogeny, using the parameter {--rec-model UndatedDL}. The species tree used is the same as
588 the one used for the phylogenetic logistic regression above. In addition to correcting the gene
589 family tree, GeneRax also reconciled it with the species tree and inferred duplication and loss
590 event counts on each branch. Tree annotation and visualization were done in R using the treeio
591 and ggtree packages (Wang et al. 2020; Yu 2020).

592 To infer the phylogenetic tree for the Hil family homologs in various *C. auris* strains and
593 infer gains and losses within species, we identified orthologs of the *HIL* genes in representative
594 strains from the four major clades of *C. auris* (B8441, B11220, B11221, B11243) (Muñoz et al.
595 2018). Orthologs from two MDR species, *C. haemuloni* and *C. pseudohaemulonis*, and from *D.*
596 *hansenii* were included to help root the tree. The gene tree was constructed as described
597 above. To root the tree, we first inferred a gene tree without the outgroup (*D. hansenii*)
598 sequences in the alignment. Then, the full alignment with the outgroup sequences along with
599 the gene tree from the first step were provided to RAxML to run the Evolutionary Placement
600 Algorithm (EPA) algorithm (Berger et al. 2011), which identified a unique root location. To
601 reconcile the gene tree with the species tree, we performed maximum likelihood-based gene
602 tree correction using GeneRax (v2.0.1) with the parameters: {--rec-model UndatedDL}. The
603 species tree was based on (Muñoz et al. 2018).

604 **Prediction for fungal adhesins and adhesin-related sequence features**

605 **1)** The potential of Hil homologs encoding fungal adhesins was assessed using FungalRV, a
606 Support Vector Machine-based fungal adhesin predictor (Chaudhuri et al. 2011). Proteins
607 passing the recommended cutoff of 0.511 were considered positive. **2)** Signal Peptide was
608 predicted using the SignalP 6.0 server, with the "organism group" set to Eukarya. The server
609 reported the proteins that had predicted signal peptides. No further filtering was done. **3)** GPI-

610 anchor was predicted using PredGPI using the General Model. Proteins with a false positive
611 rate of 0.01 or less were considered as containing a GPI-anchor. **4)** Tandem repeats were
612 identified using XSTREAM with the following parameters: {-i.7 -l.7 -g3 -e2 -L15 -z -Asub.txt -B -
613 O}, where the "sub.txt" was provided by the software package. **5)** β-aggregation prone
614 sequences were predicted using TANGO v2.3.1 with the following parameters: {ct="N" nt="N"
615 ph="7.5" te="298" io="0.1" tf="0" stab="-10" conc="1" seq="SEQ"}. **6)** Serine and Threonine
616 content in proteins were quantified using `freak` from the EMBOSS suite, with a sliding window
617 of 100 or 50 aa and a step size of 10 aa. To compare with proteome-wide distribution of Ser/Thr
618 frequency, the protein sequences for *C. albicans* (SC5314), *C. glabrata* (CBS138) and *C. auris*
619 (B11221) were downloaded from NCBI Assembly database (IDs in Table S7) and the frequency
620 of serine and threonine residues were counted for each protein. **7)** O-linked and N-linked
621 glycosylations were predicted using NetOGlyc (v4.0) and NetNGlyc (v1.0) servers.

622 **Structural prediction and visualization for the Hyphal_reg_CWP domain**

623 To perform structural predictions using AlphaFold2, we used the Google Colab notebook
624 (https://colab.research.google.com/github/deepmind/alphafold/blob/main/notebooks/AlphaFold.i
625 pynb) authored by the DeepMind team. This is a reduced version of the full AlphaFold version 2
626 in that it searches a selected portion of the environmental BFD database, and doesn't use
627 templates. The Amber relaxation step is included, and no other parameters other than the input
628 sequences are required. DALI was used to search for similar structures in the PDB50 database.
629 Model visualization and annotation were done in PyMol v2.5.2. Secondary structure prediction
630 for *C. auris* Hil1's central domain was performed using PSIPred.

631 **Dotplot**

632 To determine the self-similarity and similarity between the eight *C. auris* Hil proteins, we made
633 dotplots using JDotter (Brodie et al. 2004). The window size and contrast settings were labeled
634 in the legends for the respective plots. The self-alignment for *C. auris* Hil1 tandem repeats was
635 visualized using Jalview v2.11.

636 **Identification of intraspecific tandem repeat copy number variations among *C. auris* strains**

637 To identify polymorphisms in Hil1-Hil4 in diverse *C. auris* strains, we downloaded the genome
638 sequences for the following strains from NCBI: Clade I - B11205, B13916; Clade II - B11220,
639 B12043, B13463; Clade III - B11221, B12037, B12631, B17721; Clade IV - B11245, B12342
640 (Table S4). The amino acid sequences for Hil1-Hil4 from the strain B8441 were used as the
641 query to search the nucleotide sequences of the above assemblies using TBLASTN, with the
642 following parameters {-db_gencode 12 -evalue 1e-150 -max_hsps 2}. Orthologs in each strain

643 were curated based on the BLAST hits to either the Hyphal_reg_CWP domain alone or the
644 entire protein query. All Clade II strains had no hits for Hil1-Hil4. Several strains in Clade I, III
645 and IV were found to lack one or more Hil proteins (Table S5). But upon further inspection, it
646 was found that they had significant TBLASTN hits for part of the query, e.g., the central domain,
647 and the hits were located at the end of a chromosome, suggesting the possibility of incomplete
648 or misassembled sequences. Further experiments will be needed to determine if those *HIL*
649 genes are present in those strains.

650 **Estimation of dN/dS ratios and model comparisons**

651 We used `codeml` in PAML (v4.9e) to perform evolutionary inferences on the Hyphal_reg_CWP
652 domain in *C. auris*. We first used Clustal Omega to align the amino acid sequences for the
653 Hyphal_reg_CWP domain from Hil1-Hil8 from *C. auris* similar to how we generated the multiple
654 sequence alignment for all Hil proteins. A closely related outgroup (XP_018709340.1 from *M.*
655 *bicuspidata*) was included to root the tree. We then generated a coding sequence alignment
656 from the protein alignment using PAL2NAL (Suyama et al. 2006). We used GARD (Kosakovsky
657 Pond et al. 2006) to analyze the coding sequence alignment to detect gene conversion events.
658 The web service of GARD on datamonkey.org was run with the following parameters: {data
659 type: nucleotide, run mode: normal, genetic code: yeast alternative nuclear, site-to-site rate
660 variation: general discrete, rate classes: 3}. Based on the results, we identified two putatively
661 non-recombining partitions, P1 = 1-414 and P2 = 697-981 (the numbers refer to the alignment
662 columns). We then separately analyzed the two partitions in PAML. To test hypotheses about
663 positive selection on a subset of the sites on all branches, we compared models M2a vs M1a,
664 M8 vs M7 and M8a vs M8. The first 4 models were specified by: {seqtype = 1, CodonFreq = 1,
665 model = 0, NSsites = 0,1,2,7,8, icode = 8, fix_kappa = 0, kappa = 2, fix_omega = 0, omega =
666 0.4, cleandata = 1}. The model M8a is additionally specified by { seqtype = 1, CodonFreq = 1,
667 model = 0, NSsites = 8, fix_omega = 1 and omega = 1, cleandata = 1}. To test hypotheses for
668 variable dN/dS on different branches (no variation across sites), we used {model = 0 or 1 or 2,
669 NSsites = 0}, with the rest being the same as the site tests. Model = 0 specified the single ratio
670 model, model = 1 the free ratio model and model = 2 the user-defined model. For the user-
671 defined model, we first used estimates from the free ratio model to designate a set of branches
672 with dN/dS > 10 as the foreground and then tested if their dN/dS was significantly different from
673 the rest of the tree by comparing a two-ratio model with the single-ratio model. Since the results
674 were significant, we further tested if the foreground dN/dS was significantly greater than 1, by
675 comparing the two-ratio model to a constrained version of the model where omega was fixed at
676 1. For branch-site test, we used {model = 2, NSsites = 2, fix_omega = 0, omega = .4} as the

677 alternative model and {model = 2, NSsites = 2, fix_omega = 1, omega = 1} as the null to test for
678 positive selection on a subset of the sites on the foreground branches. Sites under positive
679 selection were identified using the Bayes Empirical Bayes (BEB) procedure, with a posterior
680 probability threshold of 0.99.

681 **Chromosomal locations of Hil family genes**

682 To compare the chromosomal locations of the Hil family genes to the background distribution,
683 we selected eight species whose genomes were assembled to a chromosomal level and are not
684 within a closely related group, including *C. albicans*, *D. hansenii*, *C. orthopsilosis*, *K. africana*, *K.*
685 *lactis*, *N. dairenensis*, *C. auris* and *C. glabrata* (Table S7). We did not include some species,
686 e.g., *C. dubliniensis*, to minimize statistical dependence due to shared ancestry. The RefSeq
687 assembly for *C. auris* was included even though it was at a scaffold level because a recent
688 study showed that seven of its longest scaffolds were chromosome-length, allowing the
689 mapping of the scaffolds to chromosomes (Muñoz et al. 2021, Supplementary Table 1). To
690 determine the chromosomal locations of the Hil homologs in these eight species, we used
691 Rentrez v1.2.3 (Winter 2017) in R to retrieve their chromosome ID and coordinates. To calculate
692 the background gene density on each chromosome, we downloaded the feature tables for the
693 eight assemblies from the NCBI assembly database and calculated the location of each gene as
694 its start coordinate divided by the chromosome length. To compare the chromosomal location of
695 the Hil family genes to the genome background, we divided each chromosome into five equal-
696 sized bins based on the physical distance to the nearest chromosomal end. We calculated the
697 proportion of genes residing in each bin for the Hil family or for all protein coding genes. To
698 determine if the two distributions differ significantly from one another, we performed a
699 goodness-of-fit test using either a Log Likelihood Ratio (LLR) test or a Chi-Squared test, as
700 implemented in the XNomial package in R (Engels 2015). The LLR test *P*-value was reported.

701 ## Acknowledgement

702 We thank members of the Gene Regulatory Evolution lab for discussion. We thank Yong Zhang
703 (CAS Zoology Institute), Peter Lipke (Brooklyn College), John McCutcheon (ASU), Matthew
704 Hahn (Indiana University), Rich Lenski (MSU), Josep Comeron (University of Iowa), Dan Weeks
705 (University of Iowa), Lois Hoyer (UIUC) and two other anonymous reviewers for providing useful
706 suggestions and critical comments. We apologize to those who have provided help and whose
707 names were not mentioned. Dr. Bin Z. He is supported by NIH R35GM137831. Lindsey F.
708 Snyder was supported by the NIH Predoctoral Training grant T32GM008629. Rachel A. Smoak

is supported by an NSF Graduate Research Fellowship Program under Grant No. 1546595, with additional support through the NSF Division of Graduate Education under Grant No. 1633098.

Reference

Ai W, Bertram PG, Tsang CK, Chan TF, Zheng XFS. 2002. Regulation of subtelomeric silencing during stress response. *Mol. Cell* 10:1295–1305.

Alsteens D, Garcia MC, Lipke PN, Dufrêne YF. 2010. Force-induced formation and propagation of adhesion nanodomains in living fungal cells. *Proc. Natl. Acad. Sci. U. S. A.* 107:20744–20749.

Anderson MZ, Wigen LJ, Burrack LS, Berman J. 2015. Real-Time Evolution of a Subtelomeric Gene Family in Candida albicans. *Genetics* 200:907–919.

Bailey DA, Feldmann PJ, Bovey M, Gow NA, Brown AJ. 1996. The Candida albicans HYR1 gene, which is activated in response to hyphal development, belongs to a gene family encoding yeast cell wall proteins. *J. Bacteriol.* 178:5353–5360.

Bates S, de la Rosa JM, MacCallum DM, Brown AJP, Gow NAR, Odds FC. 2007. Candida albicans Iff11, a secreted protein required for cell wall structure and virulence. *Infect. Immun.* 75:2922–2928.

Berger SA, Krompass D, Stamatakis A. 2011. Performance, accuracy, and Web server for evolutionary placement of short sequence reads under maximum likelihood. *Syst. Biol.* 60:291–302.

Boisramé A, Cornu A, Da Costa G, Richard ML. 2011. Unexpected role for a serine/threonine-rich domain in the Candida albicans Iff protein family. *Eukaryot. Cell* 10:1317–1330.

Bosco G, Haber JE. 1998. Chromosome break-induced DNA replication leads to nonreciprocal translocations and telomere capture. *Genetics* 150:1037–1047.

Bradley PH, Nayfach S, Pollard KS. 2018. Phylogeny-corrected identification of microbial gene families relevant to human gut colonization. *PLOS Comput. Biol.* 14:e1006242.

Brodie R, Roper RL, Upton C. 2004. JDotter: a Java interface to multiple dotplots generated by dotter. *Bioinforma. Oxf. Engl.* 20:279–281.

Brückner S, Schubert R, Kraushaar T, Hartmann R, Hoffmann D, Jelli E, Drescher K, Müller DJ, Oliver Essen L, Mösch H-U. 2020. Kin discrimination in social yeast is mediated by cell surface receptors of the Flo11 adhesin family.Brakhage AA, Barkai N, editors. *eLife* 9:e55587.

Buchan DWA, Jones DT. 2019. The PSIPRED Protein Analysis Workbench: 20 years on. *Nucleic Acids Res.* 47:W402–W407.

Butler G, Rasmussen MD, Lin MF, Santos MAS, Sakthikumar S, Munro CA, Rheinbay E, Grabherr M, Forche A, Reedy JL, et al. 2009. Evolution of pathogenicity and sexual reproduction in eight Candida genomes. *Nature* 459:657–662.

745 Camacho C, Coulouris G, Avagyan V, Ma N, Papadopoulos J, Bealer K, Madden TL. 2009.
746 BLAST+: architecture and applications. *BMC Bioinformatics* 10:421.

747 Casola C, Hahn MW. 2009. Gene conversion among paralogs results in moderate false
748 detection of positive selection using likelihood methods. *J. Mol. Evol.* 68:679–687.

749 Castaño I, Pan S-J, Zupancic M, Hennequin C, Dujon B, Cormack BP. 2005. Telomere length
750 control and transcriptional regulation of subtelomeric adhesins in Candida glabrata. *Mol.*
751 *Microbiol.* 55:1246–1258.

752 CDC. 2019. Antibiotic resistance threats in the United States, 2019. *US Dep. Health Hum. Serv.*
753 *CDC* [Internet]. Available from: https://stacks.cdc.gov/view/cdc/82532

754 Chaudhuri R, Ansari FA, Raghunandanan MV, Ramachandran S. 2011. FungalRV: adhesin
755 prediction and immunoinformatics portal for human fungal pathogens. *BMC Genomics*
756 12:192.

757 De Las Peñas A, Pan S-J, Castaño I, Alder J, Cregg R, Cormack BP. 2003. Virulence-related
758 surface glycoproteins in the yeast pathogen Candida glabrata are encoded in
759 subtelomeric clusters and subject to RAP1- and SIR-dependent transcriptional silencing.
760 *Genes Dev.* 17:2245–2258.

761 Dehullu J, Valotteau C, Herman-Bausier P, Garcia-Sherman M, Mittelviefhaus M, Vorholt JA,
762 Lipke PN, Dufrêne YF. 2019. Fluidic Force Microscopy Demonstrates That Homophilic
763 Adhesion by Candida albicans Als Proteins Is Mediated by Amyloid Bonds between
764 Cells. *Nano Lett.* 19:3846–3853.

765 Dujon B, Sherman D, Fischer G, Durrens P, Casaregola S, Lafontaine I, de Montigny J, Marck
766 C, Neuvéglise C, Talla E, et al. 2004. Genome evolution in yeasts. *Nature* 430:35–44.

767 Eberlein C, Nielly-Thibault L, Maaroufi H, Dubé AK, Leducq J-B, Charron G, Landry CR. 2017.
768 The Rapid Evolution of an Ohnolog Contributes to the Ecological Specialization of
769 Incipient Yeast Species. *Mol. Biol. Evol.* 34:2173–2186.

770 Engels B. 2015. XNomial: Exact Goodness-of-Fit Test for Multinomial Data with Fixed
771 Probabilities. Available from: https://CRAN.R-project.org/package=XNomial

772 Fagan RP, Fairweather NF. 2014. Biogenesis and functions of bacterial S-layers. *Nat. Rev.*
773 *Microbiol.* 12:211–222.

774 Fernandez-Escamilla A-M, Rousseau F, Schymkowitz J, Serrano L. 2004. Prediction of
775 sequence-dependent and mutational effects on the aggregation of peptides and
776 proteins. *Nat. Biotechnol.* 22:1302–1306.

777 Frank AT, Ramsook CB, Otoo HN, Tan C, Soybelman G, Rauceo JM, Gaur NK, Klotz SA, Lipke
778 PN. 2010. Structure and Function of Glycosylated Tandem Repeats from Candida
779 albicans Als Adhesins. *Eukaryot. Cell* 9:405–414.

780 Frieman MB, McCaffery JM, Cormack BP. 2002. Modular domain structure in the Candida
781 glabrata adhesin Epa1p, a beta1,6 glucan-cross-linked cell wall protein. *Mol. Microbiol.*
782 46:479–492.

783 Fu Y, Luo G, Spellberg BJ, Edwards JE, Ibrahim AS. 2008. Gene overexpression/suppression
784 analysis of candidate virulence factors of Candida albicans. *Eukaryot. Cell* 7:483–492.

785 Gabaldón T, Martin T, Marcet-Houben M, Durrens P, Bolotin-Fukuhara M, Lespinet O, Arnaise
786 S, Boisnard S, Aguileta G, Atanasova R, et al. 2013. Comparative genomics of emerging
787 pathogens in the Candida glabrata clade. *BMC Genomics* 14:623.

788 Gabaldón T, Naranjo-Ortíz MA, Marcet-Houben M. 2016. Evolutionary genomics of yeast
789 pathogens in the Saccharomycotina. *FEMS Yeast Res.* 16.

790 Gordon JL, Armisén D, Proux-Wéra E, ÓhÉigeartaigh SS, Byrne KP, Wolfe KH. 2011.
791 Evolutionary erosion of yeast sex chromosomes by mating-type switching accidents.
792 *Proc. Natl. Acad. Sci.* 108:20024–20029.

793 de Groot PWJ, Bader O, de Boer AD, Weig M, Chauhan N. 2013. Adhesins in human fungal
794 pathogens: glue with plenty of stick. *Eukaryot. Cell* 12:470–481.

795 Gupta R, Brunak S. 2002. Prediction of glycosylation across the human proteome and the
796 correlation to protein function. *Pac. Symp. Biocomput. Pac. Symp. Biocomput.*:310–322.

797 Hall SR, Becker CR, Duffy MA, Cáceres CE. 2010. Variation in resource acquisition and use
798 among host clones creates key epidemiological trade-offs. *Am. Nat.* 176:557–565.

799 Halme A, Bumgarner S, Styles C, Fink GR. 2004. Genetic and Epigenetic Regulation of the FLO
800 Gene Family Generates Cell-Surface Variation in Yeast. *Cell* 116:405–415.

801 Heras B, Totsika M, Peters KM, Paxman JJ, Gee CL, Jarrott RJ, Perugini MA, Whitten AE,
802 Schembri MA. 2014. The antigen 43 structure reveals a molecular Velcro-like
803 mechanism of autotransporter-mediated bacterial clumping. *Proc. Natl. Acad. Sci. U. S.*
804 *A.* 111:457–462.

805 Ho L si T, Ané C. 2014. A linear-time algorithm for Gaussian and non-Gaussian trait evolution
806 models. *Syst. Biol.* 63:397–408.

807 Ho V, Herman-Bausier P, Shaw C, Conrad KA, Garcia-Sherman MC, Draghi J, Dufrene YF,
808 Lipke PN, Rauceo JM. 2019. An Amyloid Core Sequence in the Major Candida albicans
809 Adhesin Als1p Mediates Cell-Cell Adhesion. *mBio* 10:e01766-19.

810 Holm L. 2022. Dali server: structural unification of protein families. *Nucleic Acids Res.*:gkac387.

811 Hoyer LL. 2001. The ALS gene family of Candida albicans. *Trends Microbiol.* 9:176–180.

812 HOYER LL, GREEN CB, OH S-H, ZHAO X. 2008. Discovering the Secrets of the Candida
813 albicans Agglutinin-Like Sequence (ALS) Gene Family—a Sticky Pursuit. *Med. Mycol.*
814 *Off. Publ. Int. Soc. Hum. Anim. Mycol.* 46:1–15.

815 Innan H, Kondrashov F. 2010. The evolution of gene duplications: classifying and distinguishing
816 between models. *Nat. Rev. Genet.* 11:97–108.

817 Ives AR, Garland T. 2010. Phylogenetic logistic regression for binary dependent variables. *Syst.*
818 *Biol.* 59:9–26.

819 Jenull S, Tscherner M, Kashko N, Shivarathri R, Stoiber A, Chauhan M, Petryshyn A, Chauhan
820 N, Kuchler K. 2021. Transcriptome Signatures Predict Phenotypic Variations of Candida
821 auris. *Front. Cell. Infect. Microbiol.* [Internet] 11. Available from:
822 https://www.ncbi.nlm.nih.gov/labs/pmc/articles/PMC8079977/

823 Jiang H, Bao J, Xing Y, Li X, Chen Q. 2022. Comparative Genomic Analyses Provide Insight
824 Into the Pathogenicity of Metschnikowia bicuspidata LNES0119. *Front. Microbiol.*
825 13:939141.

826 Jumper J, Evans R, Pritzel A, Green T, Figurnov M, Ronneberger O, Tunyasuvunakool K, Bates
827 R, Žídek A, Potapenko A, et al. 2021. Highly accurate protein structure prediction with
828 AlphaFold. *Nature*:1–11.

829 Kajava AV, Steven AC. 2006. The turn of the screw: variations of the abundant beta-solenoid
830 motif in passenger domains of Type V secretory proteins. *J. Struct. Biol.* 155:306–315.

831 Kean R, Delaney C, Sherry L, Borman A, Johnson EM, Richardson MD, Rautemaa-Richardson
832 R, Williams C, Ramage G. 2018. Transcriptome Assembly and Profiling of Candida auris
833 Reveals Novel Insights into Biofilm-Mediated Resistance. *mSphere* [Internet] 3.
834 Available from: https://msphere.asm.org/content/3/4/e00334-18

835 Kempf M, Cottin J, Licznar P, Lefrançois C, Robert R, Apaire-Marchais V. 2009. Disruption of
836 the GPI protein-encoding gene IFF4 of Candida albicans results in decreased adherence
837 and virulence. *Mycopathologia* 168:73–77.

838 Kosakovsky Pond SL, Posada D, Gravenor MB, Woelk CH, Frost SDW. 2006. Automated
839 Phylogenetic Detection of Recombination Using a Genetic Algorithm. *Mol. Biol. Evol.*
840 23:1891–1901.

841 Koteiche HA, Mchaourab HS. 1999. Folding pattern of the alpha-crystallin domain in alphaA-
842 crystallin determined by site-directed spin labeling. *J. Mol. Biol.* 294:561–577.

843 Kozlov AM, Darriba D, Flouri T, Morel B, Stamatakis A. 2019. RAxML-NG: a fast, scalable and
844 user-friendly tool for maximum likelihood phylogenetic inference. *Bioinforma. Oxf. Engl.*
845 35:4453–4455.

846 Kuang MC, Hutchins PD, Russell JD, Coon JJ, Hittinger CT. 2016. Ongoing resolution of
847 duplicate gene functions shapes the diversification of a metabolic network. *eLife*
848 5:e19027.

849 Kwon YJ, Shin JH, Byun SA, Choi MJ, Won EJ, Lee D, Lee SY, Chun S, Lee JH, Choi HJ, et al.
850 2019. Candida auris Clinical Isolates from South Korea: Identification, Antifungal
851 Susceptibility, and Genotyping. *J. Clin. Microbiol.* 57:e01624-18.

852 Lamoth F, Lockhart SR, Berkow EL, Calandra T. 2018. Changes in the epidemiological
853 landscape of invasive candidiasis. *J. Antimicrob. Chemother.* 73:i4–i13.

854 Levy A, Salas Gonzalez I, Mittelviefhaus M, Clingenpeel S, Herrera Paredes S, Miao J, Wang K,
855 Devescovi G, Stillman K, Monteiro F, et al. 2017. Genomic features of bacterial
856 adaptation to plants. *Nat. Genet.* 50:138–150.

857 Linder T, Gustafsson CM. 2008. Molecular phylogenetics of ascomycotal adhesins—A novel
858 family of putative cell-surface adhesive proteins in fission yeasts. *Fungal Genet. Biol.*
859 45:485–497.

860 Lipke PN. 2018. What We Do Not Know about Fungal Cell Adhesion Molecules. *J. Fungi Basel*
861 *Switz.* 4.

862 Lipke PN, Garcia MC, Alsteens D, Ramsook CB, Klotz SA, Dufrêne YF. 2012. Strengthening
863 relationships: amyloids create adhesion nanodomains in yeasts. *Trends Microbiol.*
864 20:59–65.

865 Lipke PN, Mathelié-Guinlet M, Viljoen A, Dufrêne YF. 2021. A New Function for Amyloid-Like
866 Interactions: Cross-Beta Aggregates of Adhesins form Cell-to-Cell Bonds. *Pathogens*
867 10:1013.

868 Lobley A, Sadowski MI, Jones DT. 2009. pGenTHREADER and pDomTHREADER: new
869 methods for improved protein fold recognition and superfamily discrimination.
870 *Bioinforma. Oxf. Engl.* 25:1761–1767.

871 Lockhart SR, Etienne KA, Vallabhaneni S, Farooqi J, Chowdhary A, Govender NP, Colombo
872 AL, Calvo B, Cuomo CA, Desjardins CA, et al. 2017. Simultaneous Emergence of
873 Multidrug-Resistant Candida auris on 3 Continents Confirmed by Whole-Genome
874 Sequencing and Epidemiological Analyses. *Clin. Infect. Dis. Off. Publ. Infect. Dis. Soc.*
875 *Am.* 64:134–140.

876 Louros NN, Baltoumas FA, Hamodrakas SJ, Iconomidou VA. 2016. A β-solenoid model of the
877 Pmel17 repeat domain: insights to the formation of functional amyloid fibrils. *J. Comput.*
878 *Aided Mol. Des.* 30:153–164.

879 Luo G, Ibrahim AS, Spellberg B, Nobile CJ, Mitchell AP, Fu Y. 2010. Candida albicans Hyr1p
880 Confers Resistance to Neutrophil Killing and Is a Potential Vaccine Target. *J. Infect. Dis.*
881 201:1718–1728.

882 Marcet-Houben M, Alvarado M, Ksiezopolska E, Saus E, de Groot PWJ, Gabaldón T. 2022.
883 Chromosome-level assemblies from diverse clades reveal limited structural and gene
884 content variation in the genome of Candida glabrata. *BMC Biol.* 20:226.

885 Mefford HC, Trask BJ. 2002. The complex structure and dynamic evolution of human
886 subtelomeres. *Nat. Rev. Genet.* 3:91–102.

887 Meng G, Spahich N, Kenjale R, Waksman G, St Geme JW. 2011. Crystal structure of the
888 Haemophilus influenzae Hap adhesin reveals an intercellular oligomerization mechanism
889 for bacterial aggregation. *EMBO J.* 30:3864–3874.

890 Morel B, Kozlov AM, Stamatakis A, Szöllősi GJ. 2020. GeneRax: A Tool for Species-Tree-
891 Aware Maximum Likelihood-Based Gene Family Tree Inference under Gene
892 Duplication, Transfer, and Loss. *Mol. Biol. Evol.* 37:2763–2774.

893 Muñoz JF, Gade L, Chow NA, Loparev VN, Juieng P, Berkow EL, Farrer RA, Litvintseva AP,
894 Cuomo CA. 2018. Genomic insights into multidrug-resistance, mating and virulence in
895 Candida auris and related emerging species. *Nat. Commun.* 9:5346.

896 Muñoz JF, Welsh RM, Shea T, Batra D, Gade L, Howard D, Rowe LA, Meis JF, Litvintseva AP,
897 Cuomo CA. 2021. Clade-specific chromosomal rearrangements and loss of subtelomeric
898 adhesins in Candida auris. *Genetics* [Internet]. Available from:
899 https://doi.org/10.1093/genetics/iyab029

900 Newman AM, Cooper JB. 2007. XSTREAM: A practical algorithm for identification and
901 architecture modeling of tandem repeats in protein sequences. *BMC Bioinformatics*
902 8:382.

903 Nozawa M, Suzuki Y, Nei M. 2009. Reliabilities of identifying positive selection by the branch-
904 site and the site-prediction methods. *Proc. Natl. Acad. Sci.* 106:6700–6705.

905 Oh S-H, Isenhower A, Rodriguez-Bobadilla R, Smith B, Jones J, Hubka V, Fields C, Hernandez
906 A, Hoyer LL. 2020. Pursuing Advances in DNA Sequencing Technology to Solve a
907 Complex Genomic Jigsaw Puzzle: The Agglutinin-Like Sequence (ALS) Genes of
908 Candida tropicalis. *Front. Microbiol.* 11:594531.

909 Oh S-H, Schliep K, Isenhower A, Rodriguez-Bobadilla R, Vuong VM, Fields CJ, Hernandez AG,
910 Hoyer LL. 2021. Using Genomics to Shape the Definition of the Agglutinin-Like
911 Sequence (ALS) Family in the Saccharomycetales. *Front. Cell. Infect. Microbiol.*
912 11:794529.

913 Oh S-H, Smith B, Miller AN, Staker B, Fields C, Hernandez A, Hoyer LL. 2019. Agglutinin-Like
914 Sequence (ALS) Genes in the Candida parapsilosis Species Complex: Blurring the
915 Boundaries Between Gene Families That Encode Cell-Wall Proteins. *Front. Microbiol.*
916 10:781.

917 Otoo HN, Lee KG, Qiu W, Lipke PN. 2008. Candida albicans Als Adhesins Have Conserved
918 Amyloid-Forming Sequences. *Eukaryot. Cell* 7:776–782.

919 Pierleoni A, Martelli PL, Casadio R. 2008. PredGPI: a GPI-anchor predictor. *BMC Bioinformatics*
920 9:392.

921 Potter SC, Luciani A, Eddy SR, Park Y, Lopez R, Finn RD. 2018. HMMER web server: 2018
922 update. *Nucleic Acids Res.* 46:W200–W204.

923 Qian W, Zhang JG. 2014. Genomic evidence for adaptation by gene duplication. *Genome*
924 *Res.*:gr.172098.114.

925 R Core Team. R: A Language and Environment for Statistical Computing. Vienna, Austria: R
926 Foundation for Statistical Computing Available from: https://www.R-project.org

927 Ramsook CB, Tan C, Garcia MC, Fung R, Soybelman G, Henry R, Litewka A, O'Meally S, Otoo
928 HN, Khalaf RA, et al. 2010. Yeast cell adhesion molecules have functional amyloid-
929 forming sequences. *Eukaryot. Cell* 9:393–404.

930 Rauceo JM, De Armond R, Otoo H, Kahn PC, Klotz SA, Gaur NK, Lipke PN. 2006. Threonine-
931 rich repeats increase fibronectin binding in the Candida albicans adhesin Als5p.
932 *Eukaryot. Cell* 5:1664–1673.

933 Reid SD, Herbelin CJ, Bumbaugh AC, Selander RK, Whittam TS. 2000. Parallel evolution of
934 virulence in pathogenic Escherichia coli. *Nature* 406:64–67.

935 Reithofer V, Fernández-Pereira J, Alvarado M, de Groot P, Essen L-O. 2021. A novel class of
936 Candida glabrata cell wall proteins with β-helix fold mediates adhesion in clinical
937 isolates. *PLoS Pathog.* 17:e1009980.

938 Rice P, Longden I, Bleasby A. 2000. EMBOSS: the European Molecular Biology Open Software
939 Suite. *Trends Genet. TIG* 16:276–277.

940 Richard ML, Plaine A. 2007. Comprehensive Analysis of Glycosylphosphatidylinositol-Anchored
941 Proteins in Candida albicans. *Eukaryot. Cell* 6:119–133.

942 Rosiana S, Zhang L, Kim GH, Revtovich AV, Uthayakumar D, Sukumaran A, Geddes-McAlister
943 J, Kirienko NV, Shapiro RS. 2021. Comprehensive genetic analysis of adhesin proteins
944 and their role in virulence of Candida albicans. *Genetics* [Internet]. Available from:
945 https://doi.org/10.1093/genetics/iyab003

946 RStudio Team. 2021. RStudio: Integrated Development Environment for R. Boston, MA:
947 RStudio, PBC Available from: http://www.rstudio.com/

948 Sakofsky CJ, Malkova A. 2017. Break induced replication in eukaryotes: mechanisms,
949 functions, and consequences. *Crit. Rev. Biochem. Mol. Biol.* 52:395–413.

950 Schrödinger, LLC. 2021. The PyMOL Molecular Graphics System, Version 2.5.2.

951 Sequeira S, Kavanaugh D, MacKenzie DA, Šuligoj T, Walpole S, Leclaire C, Gunning AP,
952 Latousakis D, Willats WGT, Angulo J, et al. 2018. Structural basis for the role of serine-
953 rich repeat proteins from Lactobacillus reuteri in gut microbe–host interactions. *Proc.*
954 *Natl. Acad. Sci.* 115:E2706–E2715.

955 Shen X-X, Opulente DA, Kominek J, Zhou X, Steenwyk JL, Buh KV, Haase MAB, Wisecaver
956 JH, Wang M, Doering DT, et al. 2018. Tempo and Mode of Genome Evolution in the
957 Budding Yeast Subphylum. *Cell* [Internet]. Available from:
958 http://www.sciencedirect.com/science/article/pii/S0092867418313321

959 Sievers F, Wilm A, Dineen D, Gibson TJ, Karplus K, Li W, Lopez R, McWilliam H, Remmert M,
960 Söding J, et al. 2011. Fast, scalable generation of high-quality protein multiple sequence
961 alignments using Clustal Omega. *Mol. Syst. Biol.* 7:539.

962 Singh S, Uppuluri P, Mamouei Z, Alqarihi A, Elhassan H, French S, Lockhart SR, Chiller T, Jr
963 JEE, Ibrahim AS. 2019. The NDV-3A vaccine protects mice from multidrug resistant
964 Candida auris infection. *PLOS Pathog.* 15:e1007460.

965 Smukalla S, Caldara M, Pochet N, Beauvais A, Guadagnini S, Yan C, Vinces MD, Jansen A,
966 Prevost MC, Latgé J-P, et al. 2008. FLO1 is a variable green beard gene that drives
967 biofilm-like cooperation in budding yeast. *Cell* 135:726–737.

968 Srivastava V, Singla RK, Dubey AK. 2018. Emerging virulence, drug resistance and future anti-
969 fungal drugs for Candida pathogens. *Curr. Top. Med. Chem.*

970 Stamatakis A. 2014. RAxML version 8: a tool for phylogenetic analysis and post-analysis of
971 large phylogenies. *Bioinformatics* 30:1312–1313.

972 Stamler R, Kappé G, Boelens W, Slingsby C. 2005. Wrapping the α-Crystallin Domain Fold in a
973 Chaperone Assembly. *J. Mol. Biol.* 353:68–79.

974 Steentoft C, Vakhrushev SY, Joshi HJ, Kong Y, Vester-Christensen MB, Schjoldager KT-BG,
975 Lavrsen K, Dabelsteen S, Pedersen NB, Marcos-Silva L, et al. 2013. Precision mapping
976 of the human O-GalNAc glycoproteome through SimpleCell technology. *EMBO J.*
977 32:1478–1488.

978 Steenwyk JL, Buida TJ, Li Y, Shen X-X, Rokas A. 2020. ClipKIT: A multiple sequence alignment
979 trimming software for accurate phylogenomic inference. *PLoS Biol.* 18:e3001007.

980 Suyama M, Torrents D, Bork P. 2006. PAL2NAL: robust conversion of protein sequence
981 alignments into the corresponding codon alignments. *Nucleic Acids Res.* 34:W609-612.

982 Teufel F, Almagro Armenteros JJ, Johansen AR, Gíslason MH, Pihl SI, Tsirigos KD, Winther O,
983 Brunak S, von Heijne G, Nielsen H. 2022. SignalP 6.0 predicts all five types of signal
984 peptides using protein language models. *Nat. Biotechnol.* 40:1023–1025.

985 Teunissen AW, Steensma HY. 1995. Review: the dominant flocculation genes of
986 Saccharomyces cerevisiae constitute a new subtelomeric gene family. *Yeast Chichester*
987 *Engl.* 11:1001–1013.

988 Uppuluri P, Lin L, Alqarihi A, Luo G, Youssef EG, Alkhazraji S, Yount NY, Ibrahim BA, Bolaris
989 MA, Edwards JE, et al. 2018. The Hyr1 protein from the fungus Candida albicans is a
990 cross kingdom immunotherapeutic target for Acinetobacter bacterial infection. *PLoS*
991 *Pathog.* [Internet] 14. Available from:
992 https://www.ncbi.nlm.nih.gov/pmc/articles/PMC5963808/

993 Verstrepen KJ, Jansen A, Lewitter F, Fink GR. 2005. Intragenic tandem repeats generate
994 functional variability. *Nat. Genet.* 37:986–990.

995 Verstrepen KJ, Reynolds TB, Fink GR. 2004. Origins of variation in the fungal cell surface. *Nat.*
996 *Rev. Microbiol.* 2:533–540.

997 Wang L-G, Lam TT-Y, Xu S, Dai Z, Zhou L, Feng T, Guo P, Dunn CW, Jones BR, Bradley T, et
998 al. 2020. Treeio: An R Package for Phylogenetic Tree Input and Output with Richly
999 Annotated and Associated Data. *Mol. Biol. Evol.* 37:599–603.

1000 Wasmer C, Lange A, Melckebeke HV, Siemer AB, Riek R, Meier BH. 2008. Amyloid Fibrils of
1001 the HET-s(218–289) Prion Form a β Solenoid with a Triangular Hydrophobic Core.
1002 *Science* [Internet]. Available from:
1003 https://www.science.org/doi/abs/10.1126/science.1151839

1004 Waterhouse AM, Procter JB, Martin DMA, Clamp M, Barton GJ. 2009. Jalview Version 2--a
1005 multiple sequence alignment editor and analysis workbench. *Bioinforma. Oxf. Engl.*
1006 25:1189–1191.

1007 Welsh RM, Sexton DJ, Forsberg K, Vallabhaneni S, Litvintseva A. 2019. Insights into the
1008 Unique Nature of the East Asian Clade of the Emerging Pathogenic Yeast Candida
1009 auris. *J. Clin. Microbiol.* 57:e00007-19.

1010 Wilkins M, Zhang N, Schmid J. 2018. Biological Roles of Protein-Coding Tandem Repeats in the
1011 Yeast Candida Albicans. *J. Fungi* 4:78.

1012 Willaert R. 2018. Adhesins of Yeasts: Protein Structure and Interactions. *J. Fungi* 4:119.

1013 Willbold D, Strodel B, Schröder GF, Hoyer W, Heise H. 2021. Amyloid-type Protein Aggregation
1014 and Prion-like Properties of Amyloids. *Chem. Rev.* 121:8285–8307.

1015 Winter DJ. 2017. rentrez: an R package for the NCBI eUtils API. *R J.* 9:520–526.

1016 Xie X, Qiu W-G, Lipke PN. 2011. Accelerated and adaptive evolution of yeast sexual adhesins.
1017 *Mol. Biol. Evol.* 28:3127–3137.

1018 Xu Z, Green B, Benoit N, Schatz M, Wheelan S, Cormack B. 2020. De novo genome assembly
1019 of Candida glabrata reveals cell wall protein complement and structure of dispersed
1020 tandem repeat arrays. *Mol. Microbiol.*

1021 Xu Z, Green B, Benoit N, Sobel JD, Schatz MC, Wheelan S, Cormack BP. 2021. Cell wall
1022 protein variation, break-induced replication, and subtelomere dynamics in Candida
1023 glabrata. *Mol. Microbiol.*

1024 Yang J, Yan R, Roy A, Xu D, Poisson J, Zhang Y. 2015. The I-TASSER Suite: protein structure
1025 and function prediction. *Nat. Methods* 12:7–8.

1026 Yang Z. 1998. Likelihood ratio tests for detecting positive selection and application to primate
1027 lysozyme evolution. *Mol. Biol. Evol.* 15:568–573.

1028 Yang Z. 2007. PAML 4: Phylogenetic Analysis by Maximum Likelihood. *Mol. Biol. Evol.*
1029 24:1586–1591.

1030 Yu G. 2020. Using ggtree to Visualize Data on Tree-Like Structures. *Curr. Protoc. Bioinforma.*
1031 69:e96.

1032 Zhang J. 2003. Evolution by gene duplication: an update. *Trends Ecol. Evol.* 18:292–298.

1033 Zhang J, Nielsen R, Yang Z. 2005. Evaluation of an Improved Branch-Site Likelihood Method
1034 for Detecting Positive Selection at the Molecular Level. *Mol. Biol. Evol.* 22:2472–2479.

1035 Zhao X, Oh S-H, Coleman DA, Hoyer LL. 2011. ALS51, a newly discovered gene in the
1036 Candida albicans ALS family, created by intergenic recombination: analysis of the gene
1037 and protein, and implications for evolution of microbial gene families. *FEMS Immunol.*
1038 *Med. Microbiol.* 61:245–257.

1039

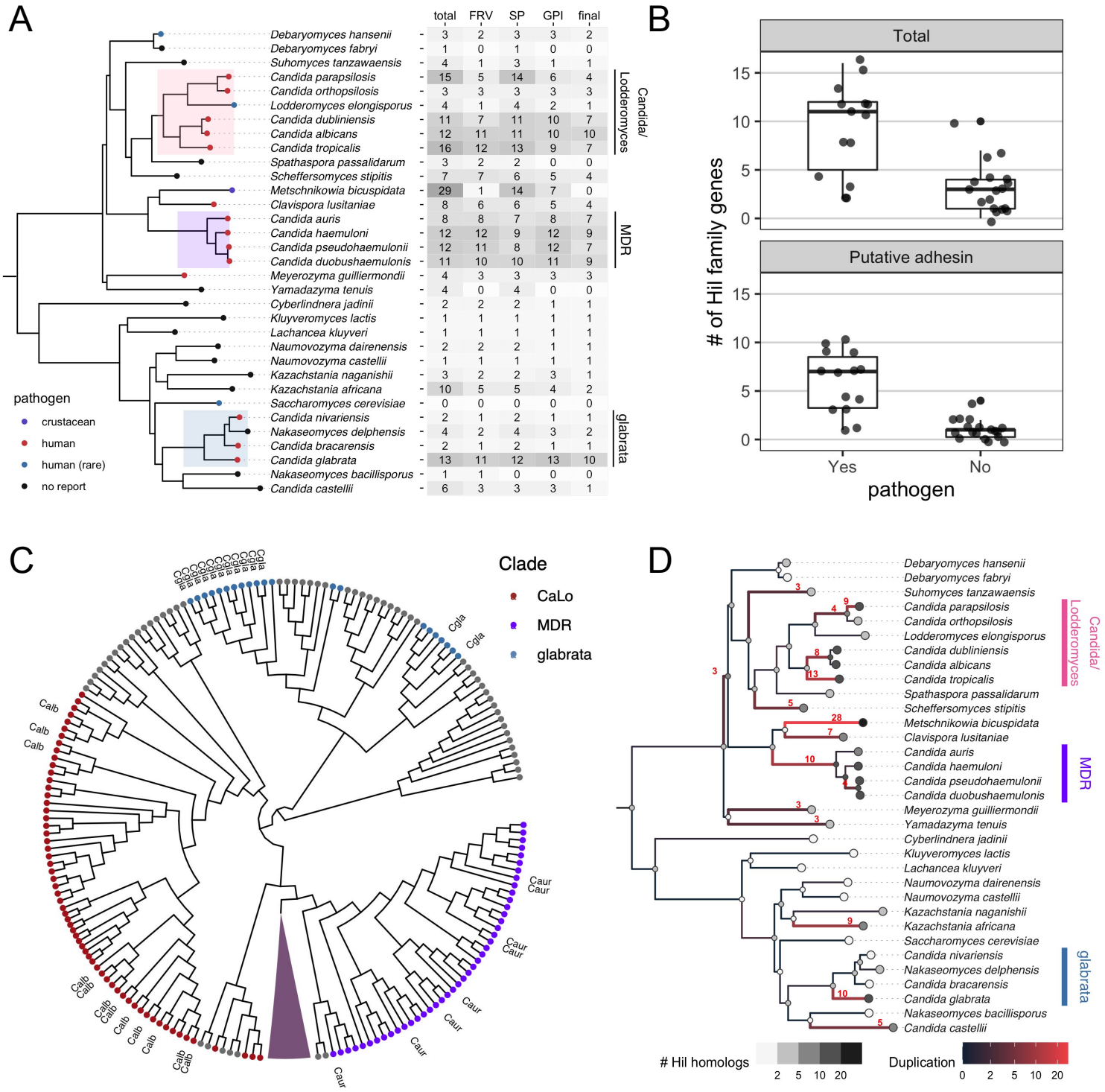

Figure 1. Phylogenetic distribution of the yeast Hil family and its parallel expansion in independently derived pathogenic *Candida* species. Legend on the next page.

Figure 1. Phylogenetic distribution of the yeast Hil family and its parallel expansion in independently derived pathogenic *Candida* species. A) Species tree is based on the phylogeny for 332 yeast species from (Shen *et al.* 2018), except for three species in the MDR clade other than *C. auris*, whose phylogenetic relationships are based on (Muñoz *et al.* 2018). The tip colors show the pathogenic status of the species. The highlighted clades are enriched in known human pathogens. In the table, the first column shows the total number of Hil family homologs per species. The number of homologs that pass each of the three tests for determining their adhesin status are shown in the next three columns. FRV = FungalRV, SP = Signal Peptide and GPI = GPI-anchor. See Materials and Methods for details. The number of homologs passing all three tests is shown in the "final" columns. (B) Boxplots comparing the number of Hil homologs (upper) or the number of putative adhesins passing all three tests (lower) per species between known pathogens and low pathogenic-potential species. Individual species numbers are shown as dots on top of the boxplot. Homologs from *M. bicuspidata* were excluded (see text). Both comparisons are significant at a 0.005 level by either a t-test with unequal variance or Mann-Whitney U test. (C) Maximum likelihood tree based on the Hyphal_reg_CWP domain of the Hil family was constructed using RAxML-NG and corrected with GeneRax based on the species tree. The tree is shown as a cladogram. All 29 homologs in *M. bicuspidata* formed a single group, which is shown as a triangle in dark plum. Homologs from the species in the three highlighted clades in (A) are colored accordingly. CaLo = Candida/Lodderomyces. Homologs from *C. albicans*, *C. auris* and *C. glabrata* are labeled as Calb, Caur and Cgla, respectively. (D) Species tree showing the number of inferred duplication events on each branch. The gray colors of the tip and internal nodes represent the identified and inferred number of Hil homologs, respectively. The branch color shows the inferred number of duplication events, with 3 or more duplications also shown as a number next to the branch.

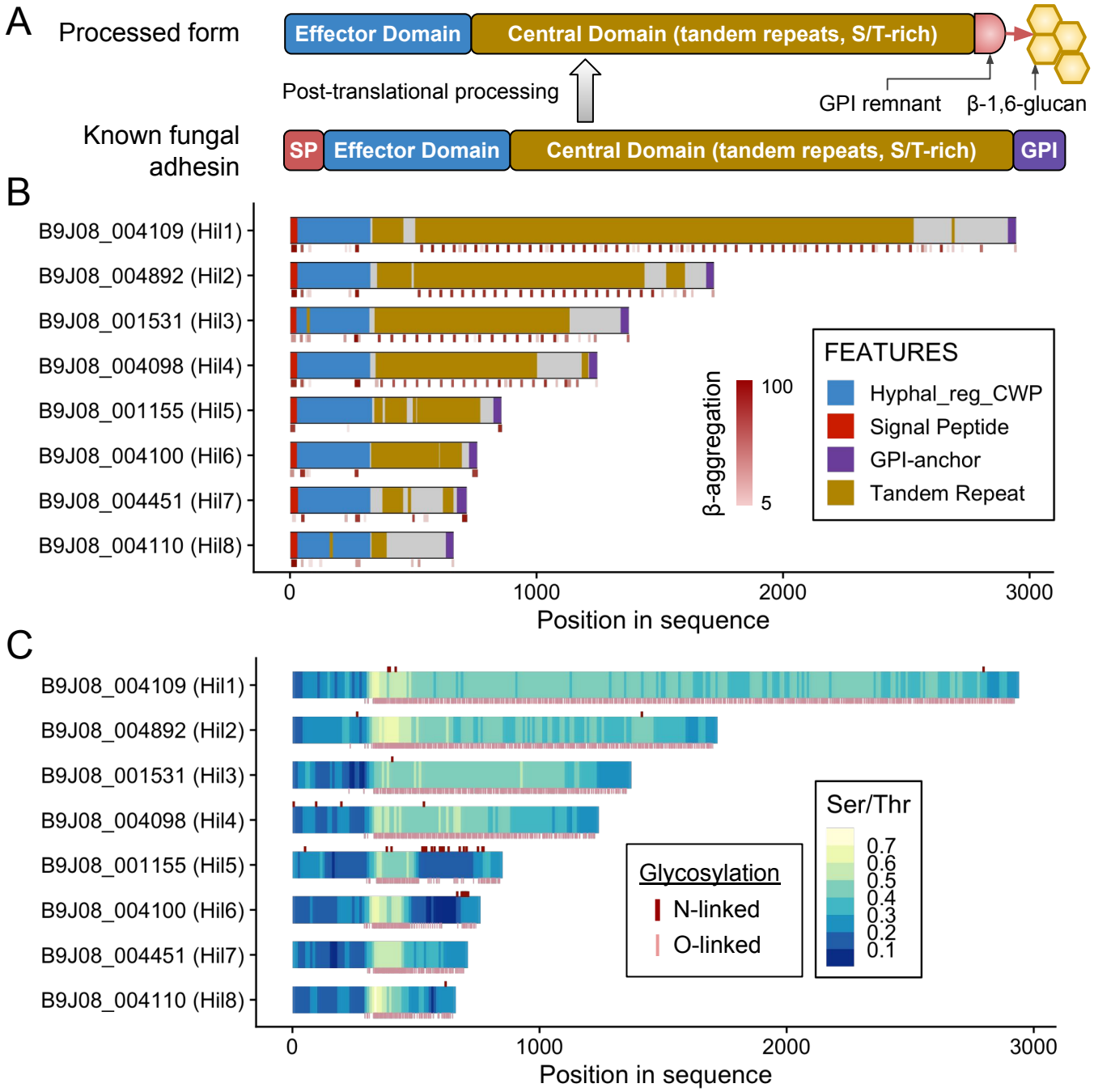

Figure 2. Domain architecture and adhesin-associated features of the *C. auris* Hil family. (A) Diagram depicting the domain organization of a typical yeast adhesin before and after the post-translational processing, adapted from (de Groot *et al.* 2013). (B) Domain features of the eight Hil proteins in *C. auris* (strain B8441). Gene IDs and names are labeled on the left. The short stripes below each diagram are the TANGO predicted β-aggregation prone sequences, with the intensity of the color corresponding to the score of the prediction. (C) Serine and Threonine (Ser/Thr) frequencies in each protein are plotted in 50 aa sliding windows with step size of 10 aa. N-linked and O-linked glycosylation sites were predicted by NetNGlyc 1.0 and NetOGlyc 4.0, respectively, and are shown as short ticks above and below each protein schematic.

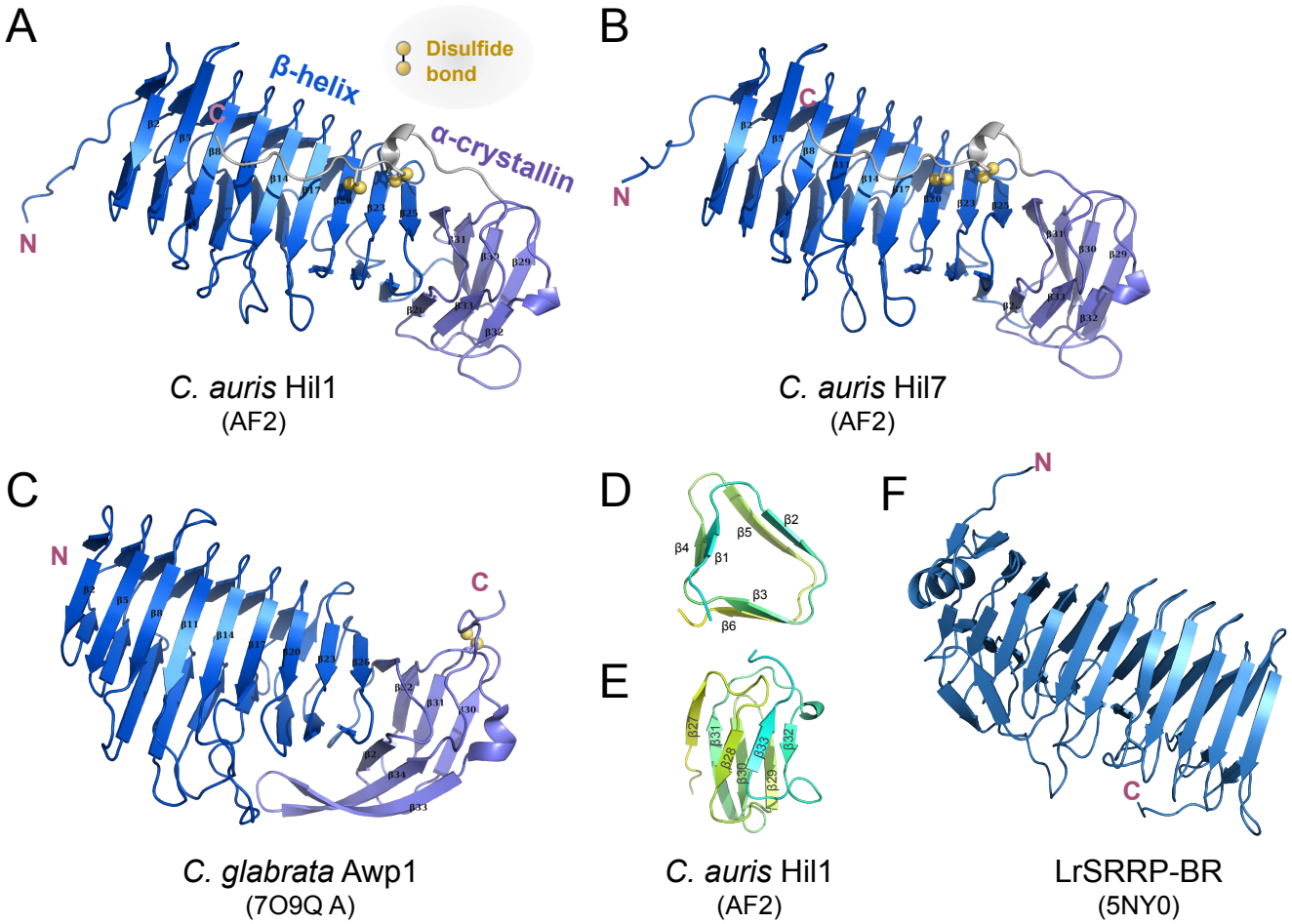

Figure 3. Predicted structures of the Hyphal_reg_CWP domain in two *C. auris* Hil proteins are similar to yeast and bacterial adhesins. (A) and (B) AlphaFold2 (AF2) predicted structures of the Hyphal_reg_CWP domains from *C. auris* Hil1 and Hil7, which consist of a β-helix followed by a α-crystallin domain, with the C-terminal loop linked to the β-helix via two disulfide bonds. (C) Crystal structure of the *C. glabrata* Awp1 effector domain, which is highly similar to *C. auris* Hil1 and Hil7, but with the disulfide bond in a different location. (D) cross-section of the first two rungs of the β-helix in (A), showing the three β-strands per rung. The cyan-to-yellow gradient follows the N- to C-terminus. (E) α-crystallin domain in (A), showing the seven β-strands forming two antiparallel β-sheets. Color is the same as in (D). (F) crystal structure of the Serine Rich Repeat Protein Binding Region (SRRP-BR) from the gram-positive bacterium *L. reuteri*, which adopts a β-helix fold.

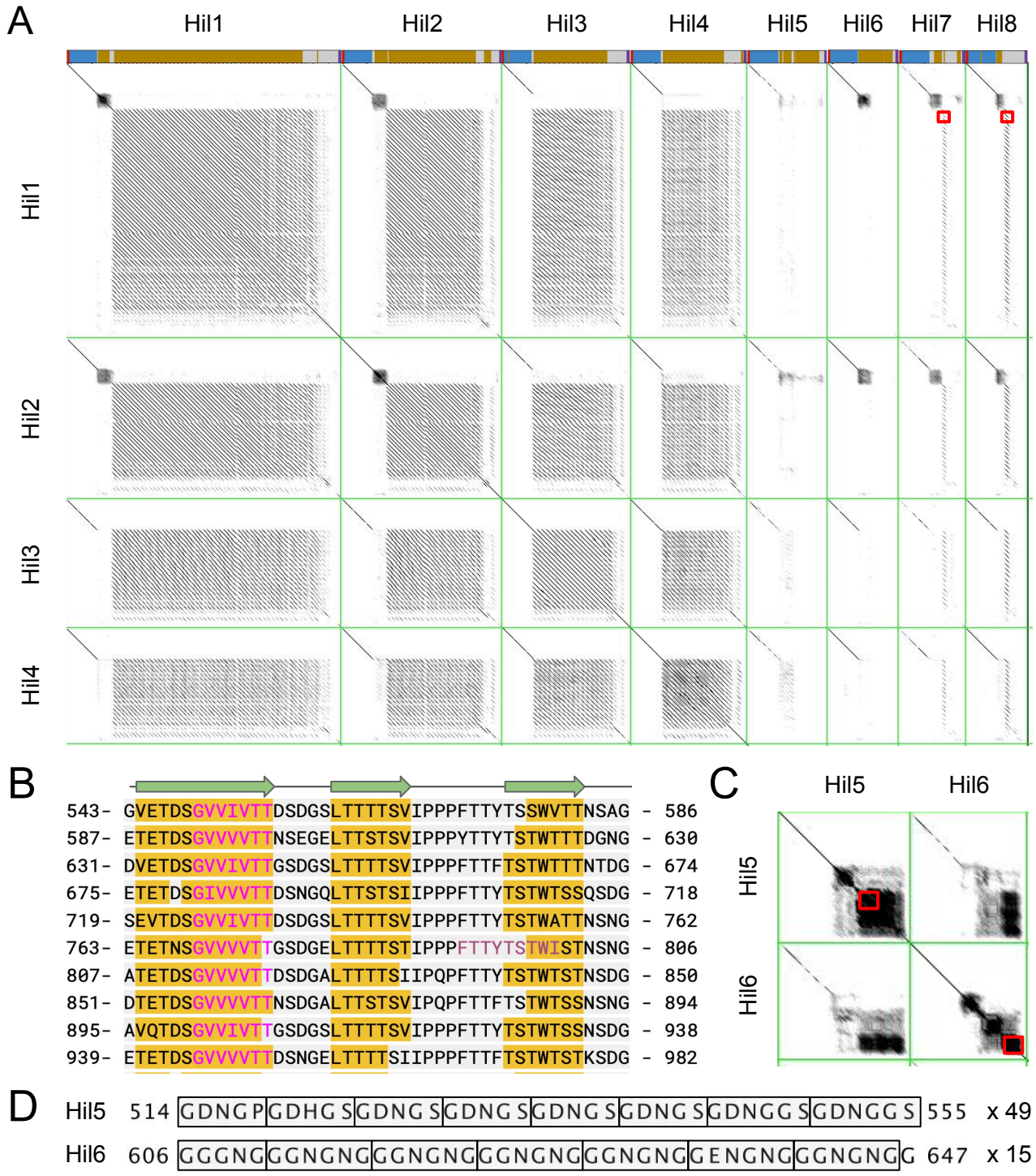

Figure 4. Dotplot shows the tandem repeat structure within and similarity between *C. auris* Hil proteins. (A) Hil1-Hil4 are compared to all eight Hil proteins in *C. auris* including themselves in dotplots (JDotter, Brodie et al 2004) with a sliding window of 50 aa and Grey Map set to 60-245 (min-max). A schematic for each protein is shown above each column (colors same as in Fig. 2). The regions highlighted by the red boxes in row 1 reveal the presence of a single copy of the 44 aa repeat unit in Hil7 and Hil8. (B) Wrapped sequence of aa 543-982 from Hil1 showing the conserved period and sequence of the 44 aa tandem repeat. The magenta and plum fonts indicate motifs predicted by TANGO to have strong (probability > 90%) or moderate (30-90%) β-aggregation potential. The yellow highlighted regions are predicted to form β-strands by PSIPred, with cartoons shown above. (C) Dotplots between Hil5 and Hil6 with the same settings as in (A), showing the low complexity repeats unique to these two. Regions within the two red boxes are shown in (D), with residue numbers shown on both ends. The rectangles delineate individual repeats, with the number of copies for each repeat shown to the right.

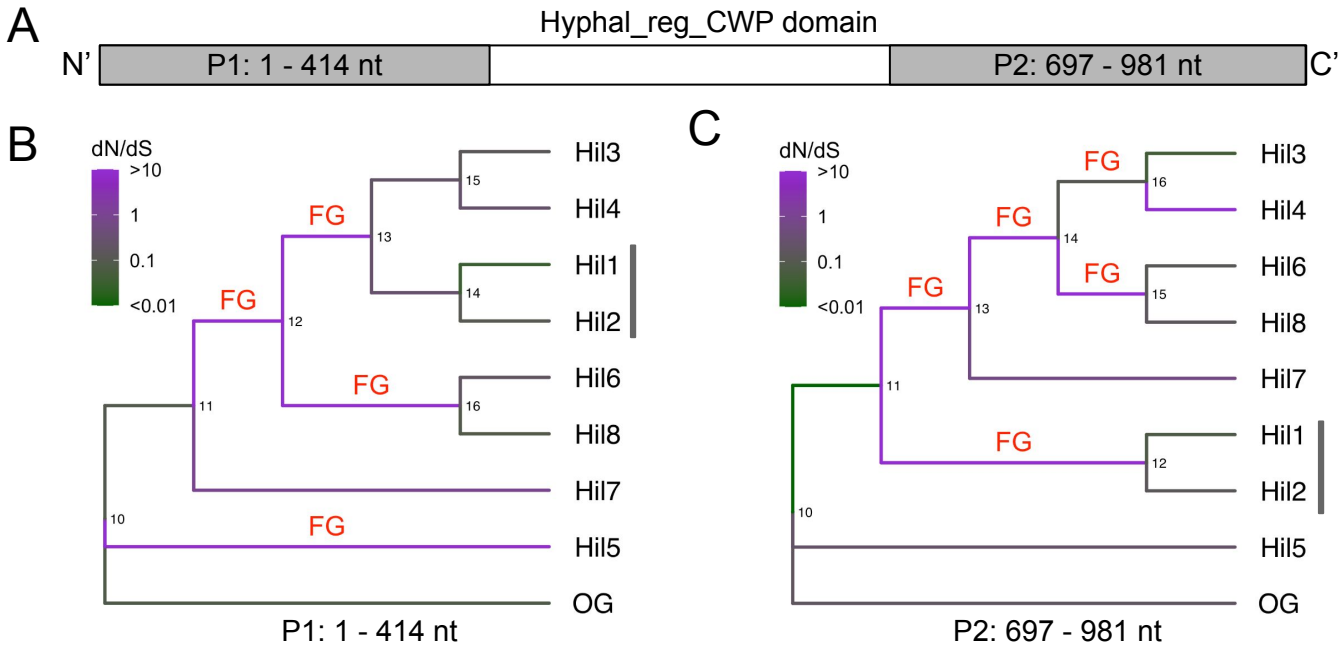

D

Tests and models compared	Partition 1-414 nt	Partition 697- 987 nt
a. branch test for variable dN/dS (=ω) between FG=foreground and the rest branches (BG)		
H_0: single dN/dS (ω) **H_1**: two dN/dS (ω_{FG} free)	$P < 0.001$ $\omega_{FG} = 1.77$, $\omega_{BG} = 0.13$	$P < 0.01$ $\omega_{FG} = 1.53$, $\omega_{BG} = 0.14$
H_0: two dN/dS (ω_{FG} == 1) **H_1**: two dN/dS (ω_{FG} free)	Insig.	Insig.
b. branch-site test for positive selection		
H_0: no positive selection **H_1**: positive selection on specific sites in the FG branches	$P < 0.01$ p(ω>1) = 0.53, ω2 = 224.43 *S39, G112*	$P < 0.01$ p(ω>1) = 0.19, ω2 = 9.85 *A234, D287, S304*

Figure 5. Maximum-likelihood-based analyses for selective pressure variation and role of positive selection on the Hyphal_reg_CWP domain in *C. auris*. (A) Schematic showing the putative non-recombining partitions within the Hyphal_reg_CWP domain determined by GARD (see Fig. S8). The two partitions labeled in gray were studied separately. The numbers refer to the columns in the coding sequence alignment. (B, C) Phylogenetic trees were reconstructed for the two partitions and are shown as a cladogram. The vertical bar next to the Hil1/Hil2 pair indicates the difference in topology between the two trees. Branch colors are based on the dN/dS values estimated from a free-ratio model in PAML. "FG" designate foreground branches, whose dN/dS were greater than 10, except for branch 14..16 in (C), which was selected instead of 16..Hil4 because this would require fewer evolutionary changes in selective forces. We also analyzed the scenario with 16..Hil4 as the foreground and the conclusions remained the same with slightly different *P*-values. (D) Summary of the maximum-likelihood-based tests for selective force heterogeneity and for positive selection. "Insig." means *P*-value > 0.05. In the branch-site test, p(ω>1) is the total proportion of sites with dN/dS > 1 on the FG branches, and ω2 their estimated dN/dS. The listed sites were identified as being under positive selection with a posterior probability greater than 0.99 by the Bayes Empirical Bayes (BEB). The one-letter code and number refer to the amino acid in the OG sequence and the alignment column (Fig S7).

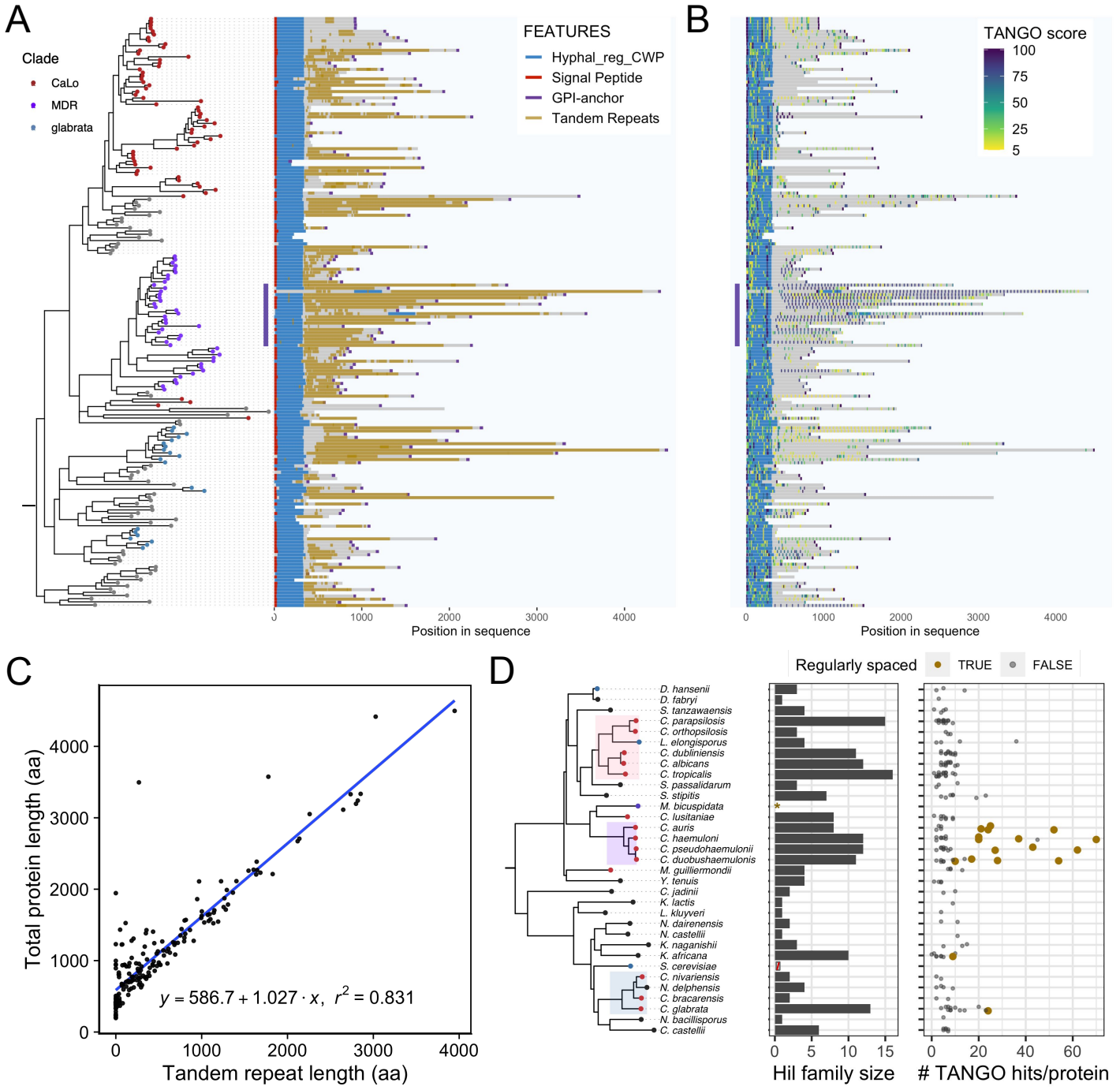

Figure 6. Evolution of protein length and β-aggregation potential in the yeast Hil family. (A) Domain schematic shows that most homologs have a signal peptide at the N-terminus, then the Hyphal_reg_CWP domain and a highly repetitive region central domain, followed by the C-terminal GPI-anchor peptide. Homologs from *M. bicuspidata* were not included because many were annotated as incomplete. They were also excluded from other results in this figure. (B) Distribution of TANGO predicted β-aggregation sequences. The score for each sequence is shown as a color gradient and represents the median of the per-residue probability of aggregation. A vertical bar marks a group of MDR clade sequences that have a large number of β-aggregation prone sequences arranged in regular intervals. (C) X-Y plot showing the relationship between total protein length and tandem repeat sequence length for Hil family homologs. The linear regression line is shown in blue, with coefficients and r^2 values below. (D) The species tree on the left is the same as in Figure 1. The middle panel shows the number of Hil homologs per species. *M. bicuspidata* homologs were excluded; *S. cerevisiae* was included in the species tree but no Hil homolog was identified in it (see text). The right panel shows the number of predicted β-aggregation prone motifs per Hil homolog. Only motifs with a median probability >= 30% were counted. Proteins are colored in gold if they have five or more such motifs and if the Median Absolute Deviation (MAD) of the inter-motif distances is < 5 aa.

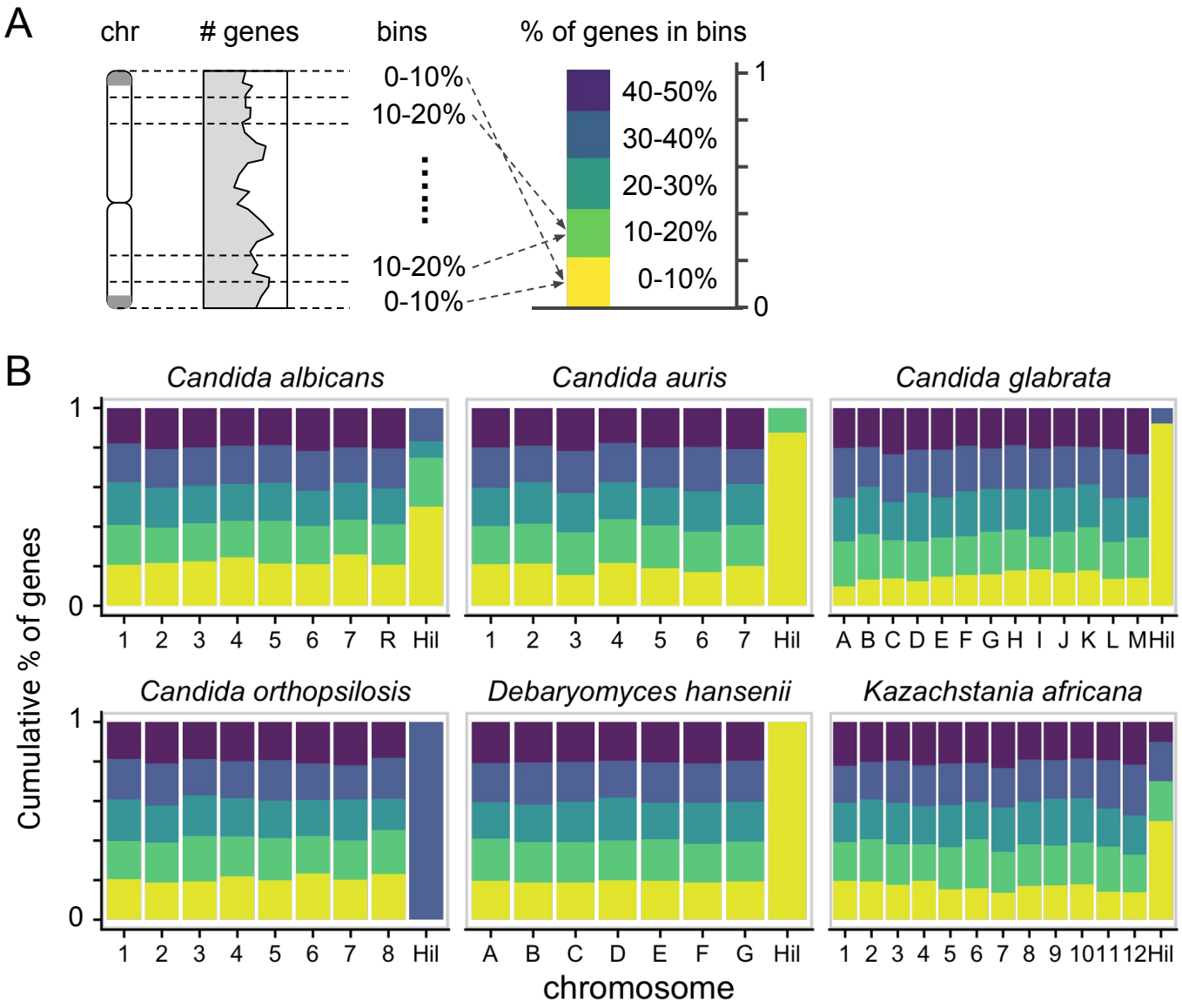

Figure 7. Hil family genes are preferentially located near the chromosome ends. (A) Schematic of the analysis: each chromosome (chr) is folded in half and divided into five equal-length "bins", ordered by their distance to the nearest telomere. The cumulative bar graph on the right summarizes the gene density distribution in the five bins. (B) Folded gene density distribution for six species with a chromosomal level assembly and more than two Hil family genes. The bin colors are as shown in (A). The Hil homologs in each species are plotted as a separate group. A goodness-of-fit test comparing the distribution of the Hil family genes to the genome background yielded a *P*-value of 1.3×10^{-12}.

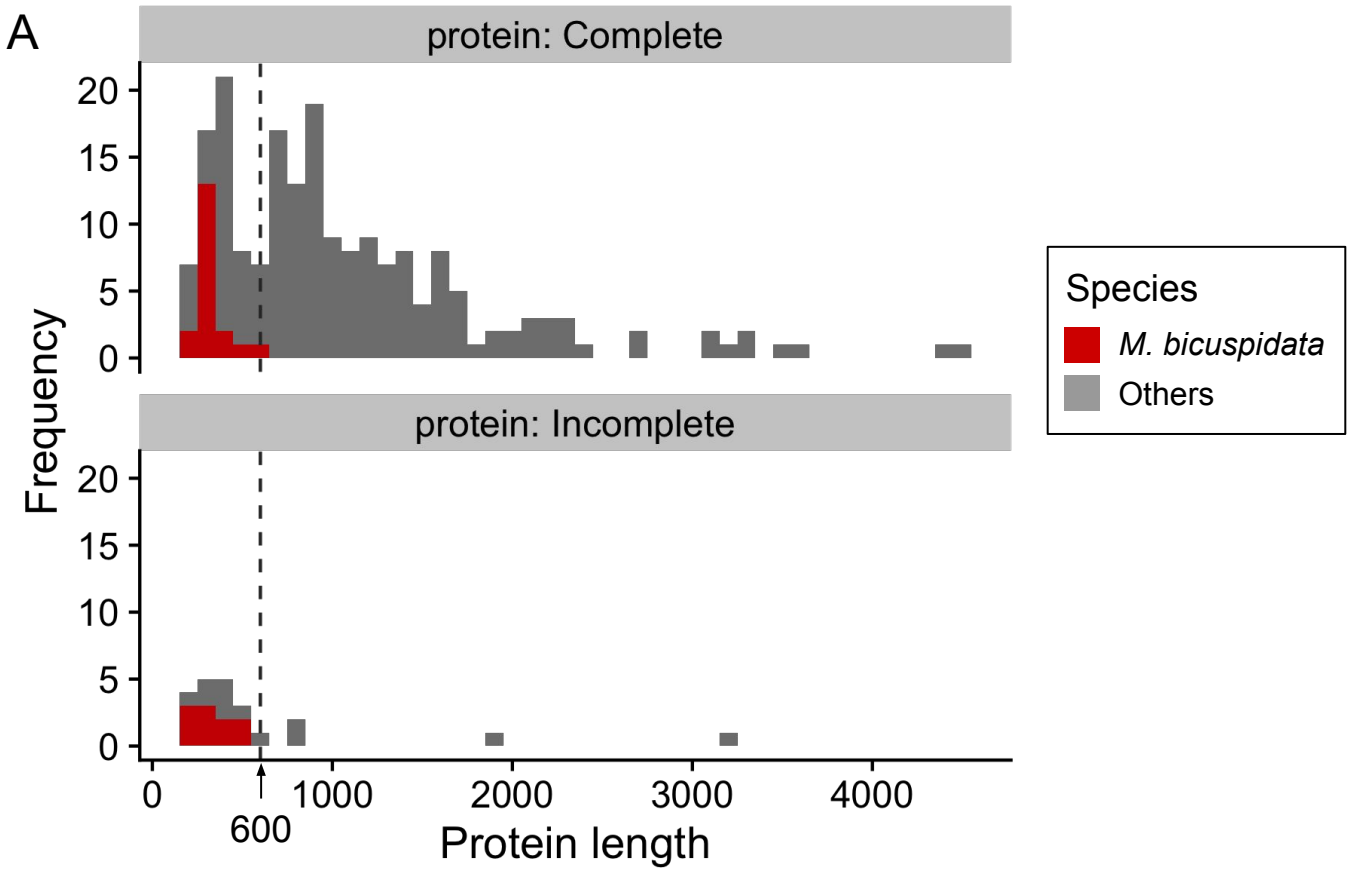

B

length	sp-gpi-	sp-GPI+	SP+gpi-	SP+GPI+	total
>600	3	14	9	112	138
251-600	12	5	27	4	48
0-250	3	0	3	1	7

Supplementary Figure 1. Hil family proteins' length distribution and grouping by signal peptide (SP) and GPI-anchor signal presence. (A) Histogram showing the distribution of protein lengths for Hil family proteins from 32 yeast species. Top: protein sequence records were labeled as complete or "NA"; bottom: proteins labeled as incomplete (no-right, no-left, no-ends). Most of the short sequences (<600 aa, dashed vertical line) came from the species *M. bicuspidata* (red) (B) Summary of the number of Hil family proteins predicted to have a signal peptide (SP+) and GPI-anchor signal (GPI+), grouped by protein length. Proteins labeled as incomplete were excluded from this table.

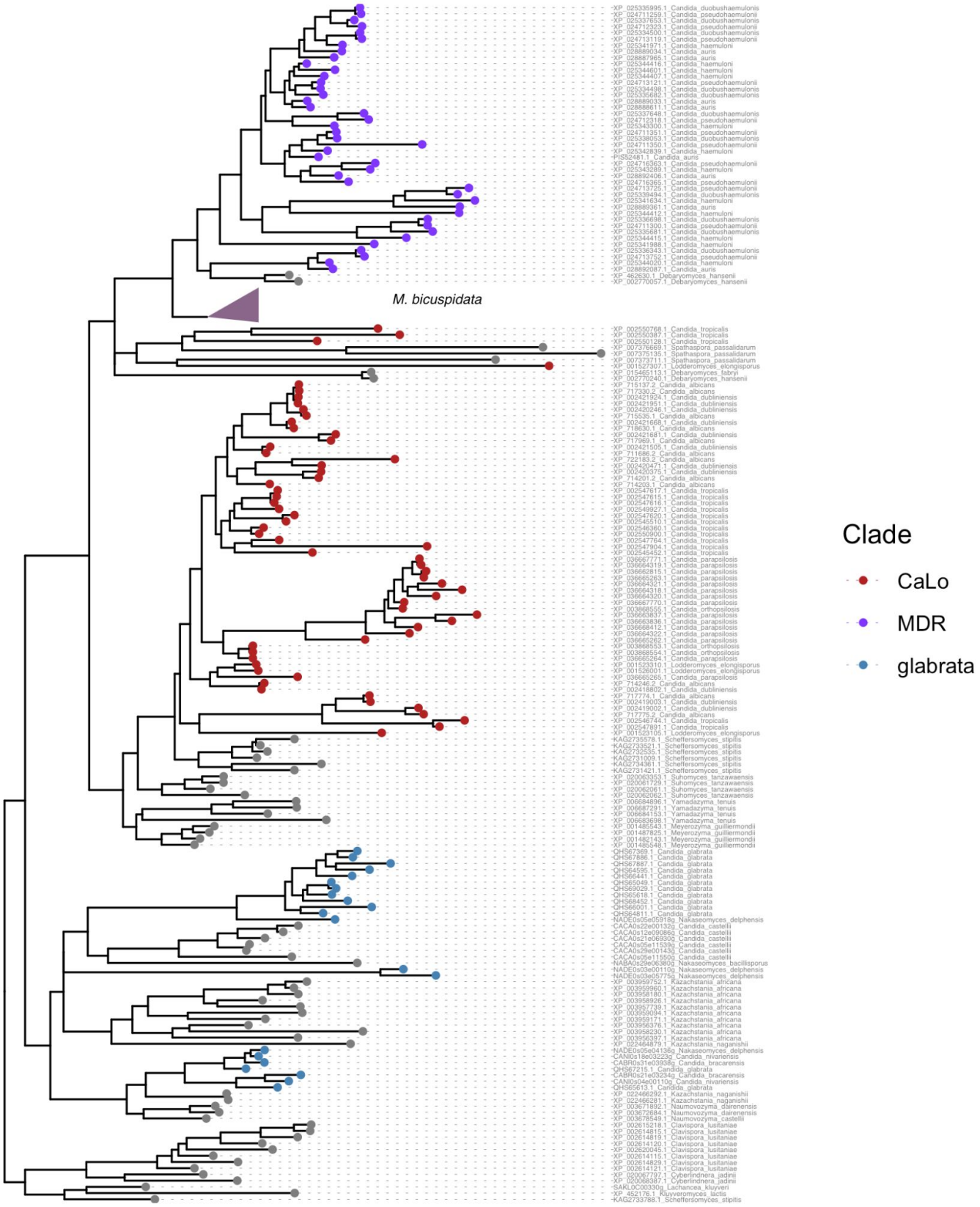

Supplementary Figure 2. Maximum likelihood tree for the Hil family genes. This tree is identical to the one shown in Fig 1C, except that it is shown in a rectangular format with the sequence names in the form of refseqID_species_name. Note that all 29 *M. bicuspidata* homologs form a single clade, which is collapsed for the ease of viewing. Their sequence IDs can be found in Table S1.

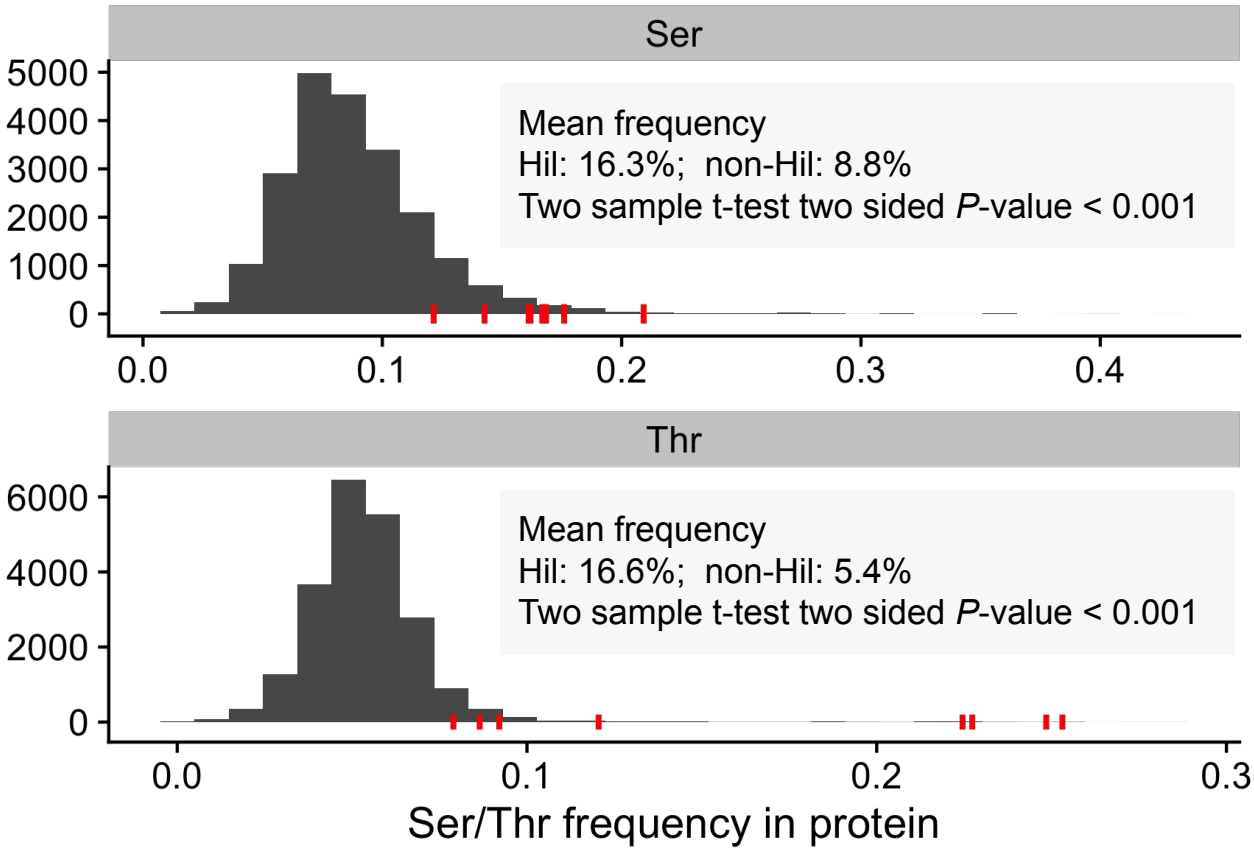

Supplementary Figure 3. Comparison of the Ser/Thr frequencies in *C. auris* Hil family members with all protein-coding genes in *C. auris*. B8441 strain genome is used for this analysis. The frequency of Ser or Thr residues as a percent of the entire protein length is plotted as a histogram for all protein-coding genes. Red ticks indicate the eight Hil genes. A student's t-test was used to assess the significance of the difference in Ser/Thr frequencies between the Hil family proteins vs the rest of the proteome.

```
1   DSGVVIVTTDSDGSLTTTTSVIPPPFTTYTSSWVTTNSAGETET
2   DSGVVVVTTNSEGELTTSTSVIPPPYTTYTSTWTTTDGNGDVET
3   DSGVVIVTTGSDGSLTTTTSVIPPPFTTFTSTWTTTNTDGETET
4   DSGIVVVTTDSNGQLTTSTSIIPPPFTTYTSTWTSSQSDGSEVT
5   DSGVVIVTTDSDGSLTTTTSVIPPPFTTYTSTWATTNSNGETET
6   NSGVVVVTTGSDGELTTTTSTIPPPFTTYTSTWISTNSNGATET
7   DSGVVVVTTDSDGALTTTTSIIPQPFTTYTSTWTSTNSDGDTET
8   DSGVVVVTTNSDGALTTSTSVIPQPFTTFTSTWTSSNSNGAVQT
9   DSGVVIVTTGSDGSLTTTTSVIPPPFTTYTSTWTSSNSDGETET
10  DSGVVVVTTDSNGELTTTTSIIPPPFTTFTSTWTSTKSDGAVET
11  DSGVIIVTTNSEGDLTTTTSIIPPPYTTYTSTWTTTDSNGVTET
12  DSGVVVVTTDSDGQLTTATSIIPPPFTTYTSTWTTTNSDGSEET
13  DSGVVIVTAGTDGSLTTTTSVIPPPFTTYTSTWITTNSNGAVET
14  DSGIIVVTTNSGGSLTTSTSVLPTPFTTYTSTWTTSDGDGNVQT
15  DSGVVIVTTGSDGALSTTTSVIPPPFTTYTSTWISTNSDGETET
16  DSGVVVVTTDSNGALTTTTSIIPPPFTTFTSTWTTTDENGATET
17  DSGVVVVTTGTDGSLTTTTSVIPPPYTTFTSTWTTSNSNGDIET
18  DSGVVIVTTNSDGSLTTTTSVIPPPYTTFTTTWATTNSDGTTET
19  DSGVVIVTTDSEGQLTTTTSVIPPPFTTYTSTWTSNKSDGAVET
20  DSGVVIVTTDSDGALTTTTSIIPQPFTTYTSTWTSTNSNGAIET
21  ESGVVVVTTDSNGALTTSTSVIPLPLTTFTTTWTTTNSAGETET
22  DSGVVVVETNSNGALTTTTSTFPEPFTTFTSTWTTTDDSGAIAT
23  DSGVVIVTTGSDGSLSTTTSVIPPPFTTYTTTWTSTNSNGGVET
24  DSGVVIVTTNSDGALETTTSVIDPPFNTYTSTWTTTDADGAIET
25  DSGVVVVTTGSDGSLTTTTSVIPHPFTTYTSTWVTTGSDGDTET
26  DSGVIVVTTDSDGALTTSTSLLPVPFTTYTSTWTITNSDGSQAT
27  DSGVVIVTTDSEGQLTTTTSVIPPPFTTYTSTWTTTGANGGEET
28  DSGVIIVTTDSDGQLATTTSVIPPPFTTFTSTWTTTNSDGNQAT
29  DSGVVIVTTDSDGQLTTTTSVIPPPFTTYTSTWTTTDGNGAEET
30  DSGVIIVTTDSEGQLTTTTSVIPPPFTTYTSTWTTTGADGSEET
31  DSGVIIVTTDSAGQLTTTTSVIPPPFTTFTSTWTTTDGNGNEGT
32  DSGVIIVTTDSDGALTTTTAVIPPAAGSGTDALSSSINDVPYTTYTSTWTTTDGNGNIET
33  DSGVVIVTTDSQGSLTTTTSIIDSPFTTYTSTWATTDNNGNVET
34  DSGVVIVTTDSNGQLTTTTSVIDSPYTTYTTSWPTTDANGGVET
35  DSGVVIVTTDSDGQLSTTTSVIDSPFTTYTTSWPTTDGNGAVET
36  DSGVVIVTTDSNGQLTTTTSVIDSPYTTYTTSWPTTGADGAVET
37  NSGVVIVTTDSDGQLTTTTSVIDSPYTTYTSIWTTTDSVGNVET
38  DSGVVIVTTDSDGQVTTTTSRFENSPSDLTEYTTTWASTDSDGNIKT
39  DSGVVVVTTDSAGSTTTSTSTFDTPYTTFTSTWTTTNGNGDVKT
40  DSGVIIVTTDSVGQLTTTTSQFDSQQSGLTDYTTTWTTTDRNGNPST
41  ASGVVVVTTDSDGQITSTTSQFSDKSSGLTDYTTTWTTTDTDGSVVT
42  DSGVVIVTTDSAGSLTTTTSVFDTPITTFTSTWTTTNADGSIET
43  DSGVIIVTADSNGQLTTTTSQSDNRPSGLTDYTTTWTTTNTDGAIET
44  DSGVVVVTTDSQGQLTTITSVIESPVTASSGSSDKPSGITEFTTTWTTTDANGIAHT
45  DSGVVIVTTDADGSLTTTTSQIDNVSSGLTEFTSSWTTTLSDGSVET
46  DSGLVIVTTDSNGQLKTTTSQFEDIPSGLSEFTTSWTTTDADGDTRI
47  DSGVVIVTTDSDNRLTTTTSQFASVDPTDFTSYITSWTATNGDGSIET
48  DSGAVIVTTNSDGQLVTTTSVISSSHGAVSTSES
49  DS-NVIVTTDSEGSLTTSTVTLCPQCTHFTSTWTTSNSEGAIET
50  DSGVVVVTTDSVGSLTTYTKDCPEASGELSTFISTYTTTDTDGNIKTT
```

Supplementary Figure 4. Tandem repeats in the *C. auris* Hil1 central domain. The majority of the 50 tandem repeat copies have a conserved 44 aa period. Dark and light orange highlights show sequences predicted by TANGO to have strong (>90%) or moderate (30-90%) β-aggregation potentials.

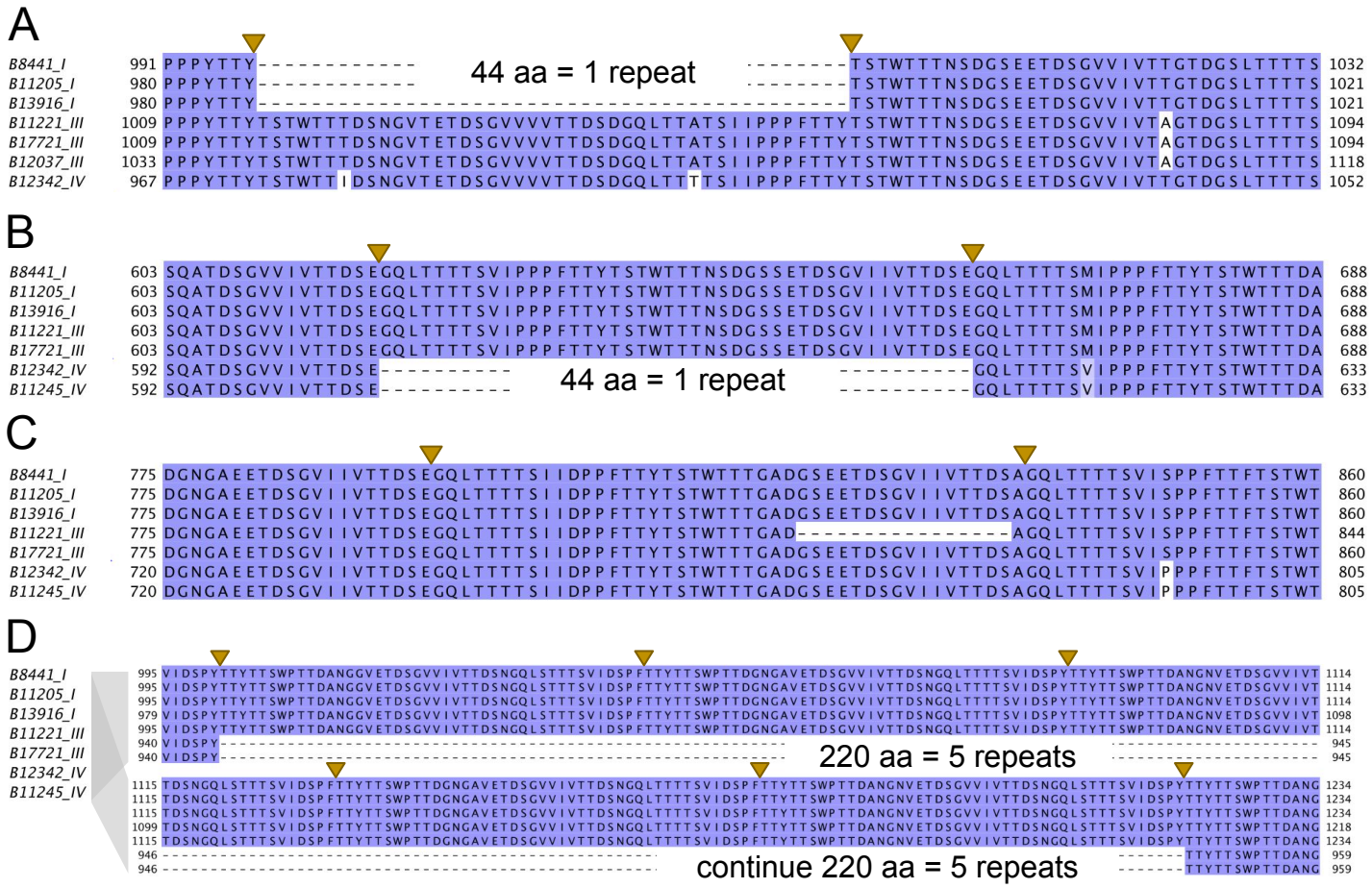

Supplementary Figure 5. Examples of tandem repeat copy number variation in Hil1-Hil4 among the *C. auris* strains. (A) A 44 aa indel in Hil1 removes exactly one repeat in all three Clade I strain orthologs. (B) A similar indel polymorphism of exactly one repeat length in Hil2 affecting the Clade IV strains. (C) An indel polymorphism in Hil2 that affects one Clade III strain and spans 16 aa, not a full repeat, but includes a predicted strong β-aggregation prone sequence “GVIIVTT”. (D) An indel polymorphism in Hil2 that spans 220 aa or five full repeats affecting the Clade IV strains. Similar patterns were observed in Hil3 and Hil4.

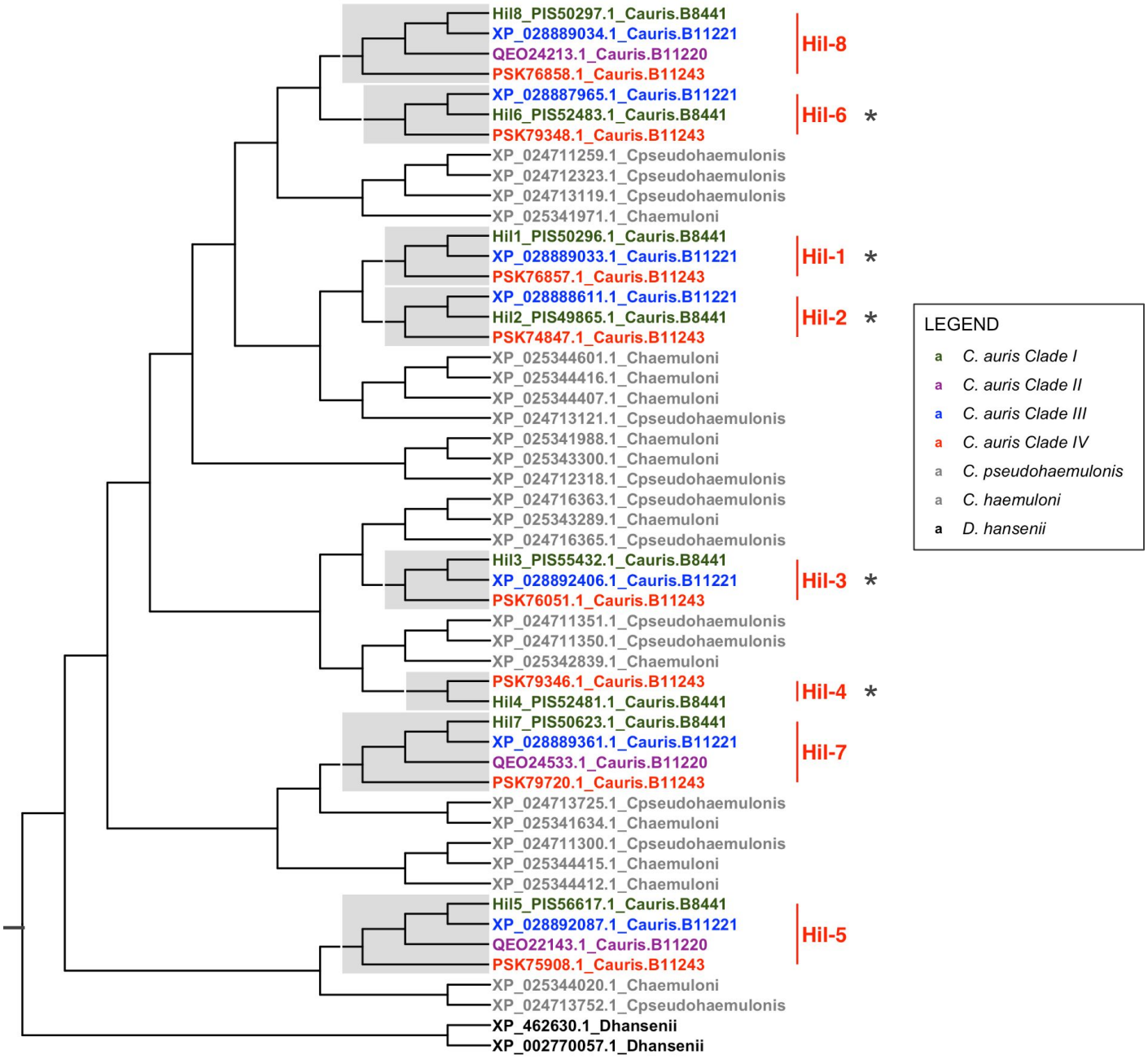

Supplementary Figure 6. Reconciled Hil family gene tree based on the Hyphal_reg_CWP domain alignment in the four clades of *C. auris* strains and two closely related species. The tree is rooted by the two homologs from the outgroup *D. hansenii*. The gene tree was corrected with the species/strain tree based on (Muñoz et al 2018) using GeneRax (v2.0.4). Hil genes lost in *C. auris* Clade II strains are labeled with an asterisk next to the Hil1-8 group labels.

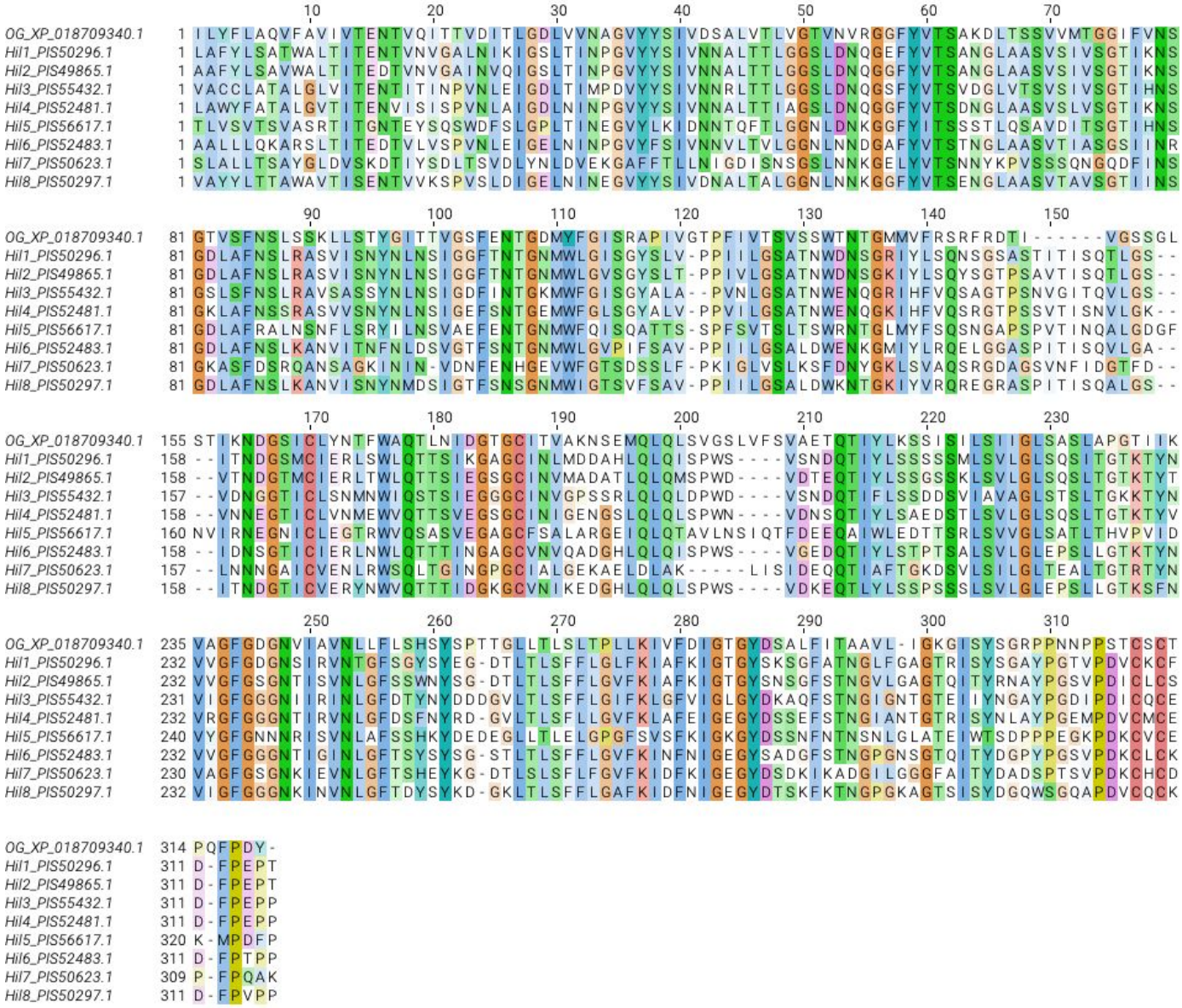

Supplementary Figure 7. Multiple sequence alignment of *C. auris* Hil1-8 Hyphal_reg_CWP domain. The domain regions were identified using HMMScan against the Pfam-A database. The sequences were aligned with clustalo v1.2.4 and the result visualized in Jalview v2.11.1.4 with the ClustalW color scheme. OG = outgroup from *M. bicuspidata*

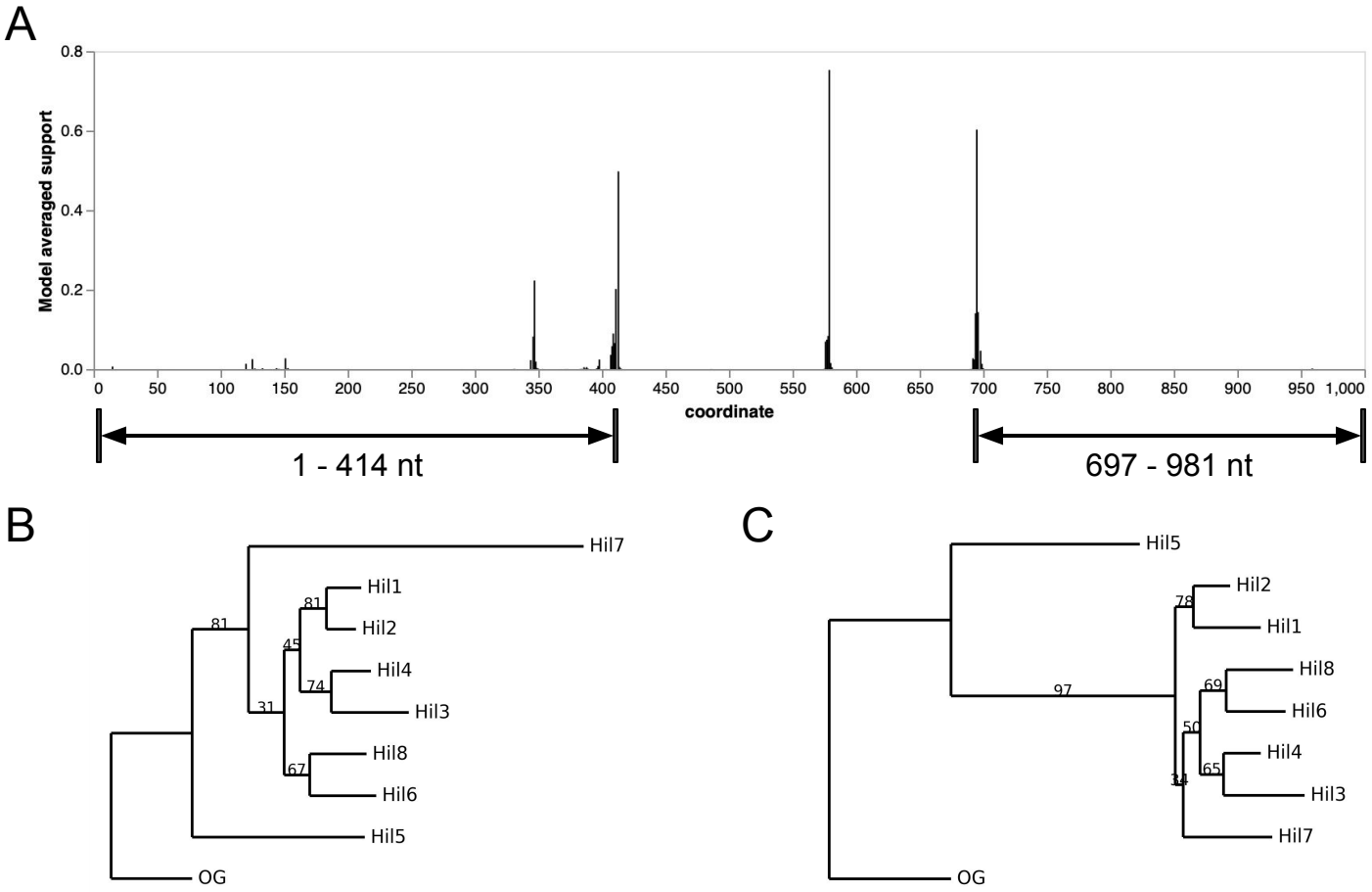

Supplementary Figure 8. Detecting intra-domain recombination and identifying non-recombining partitions in the Hyphal_reg_CWP domain using GARD. (A) Model averaged support for breakpoint locations along the Hyphal_reg_CWP domain alignment for the eight Hil proteins in *C. auris* and an outgroup sequence from *M. bicuspidata* (protein ID: XP_018709340.1) to root the gene tree. Based on the GARD output, we chose the N- and C-terminal partitions for downstream analyses, i.e., coordinates 1-414 nt and 697-981 nt. (B) A maximum likelihood tree for partition 1-414 was constructed using RAxML-NG v1.1.0. Branch length is proportional to the amount of sequence divergence. OG stands for outgroup. Bootstrap support for internal splits are shown as a percentage and are based on 1000 replicates or until bootstrapping converges. (C) tree for 697-981nt, same format as in (B)

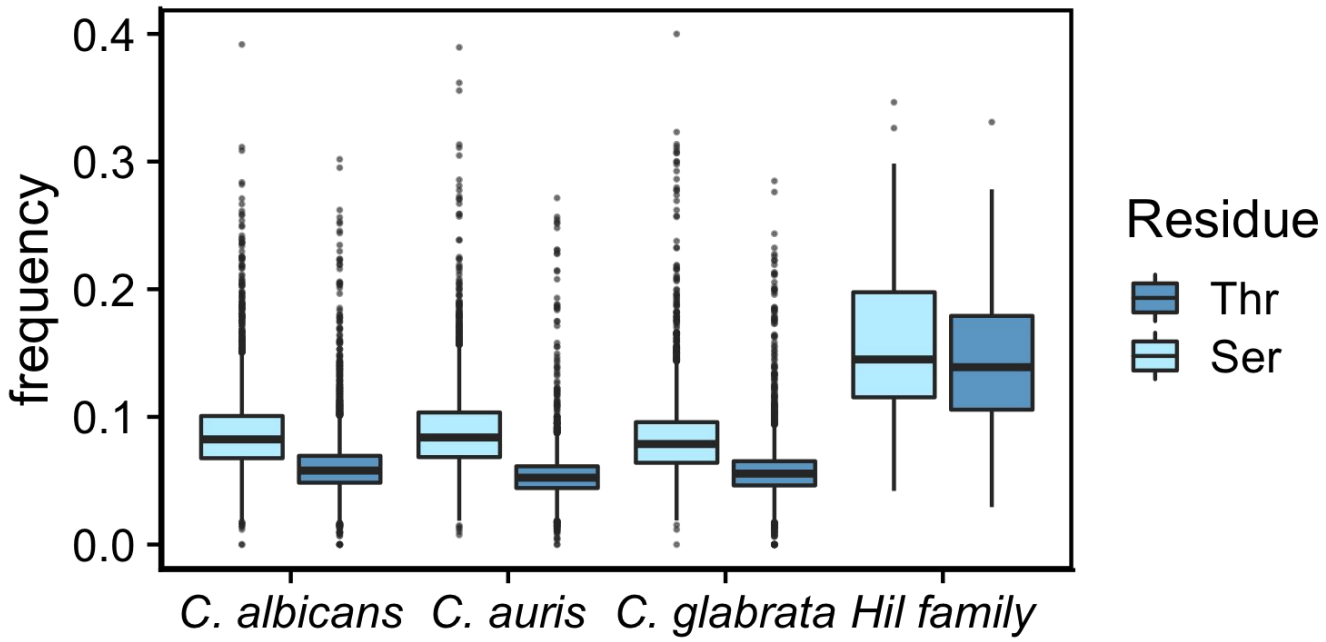

Supplementary Figure 9. Yeast Hil family proteins have on average higher Ser/Thr frequencies than the rest of the proteome. Proteome-wide distribution of Thr/Ser frequencies per protein from three species, compared with the yeast Hil family proteins (*M. bicuspidata* homologs were excluded because a large number of them were incomplete). The boxes represent the interquartile range (IQR), the middle thick line the median, the whiskers the 1.5 x IQR and the dots outliers outside that range.

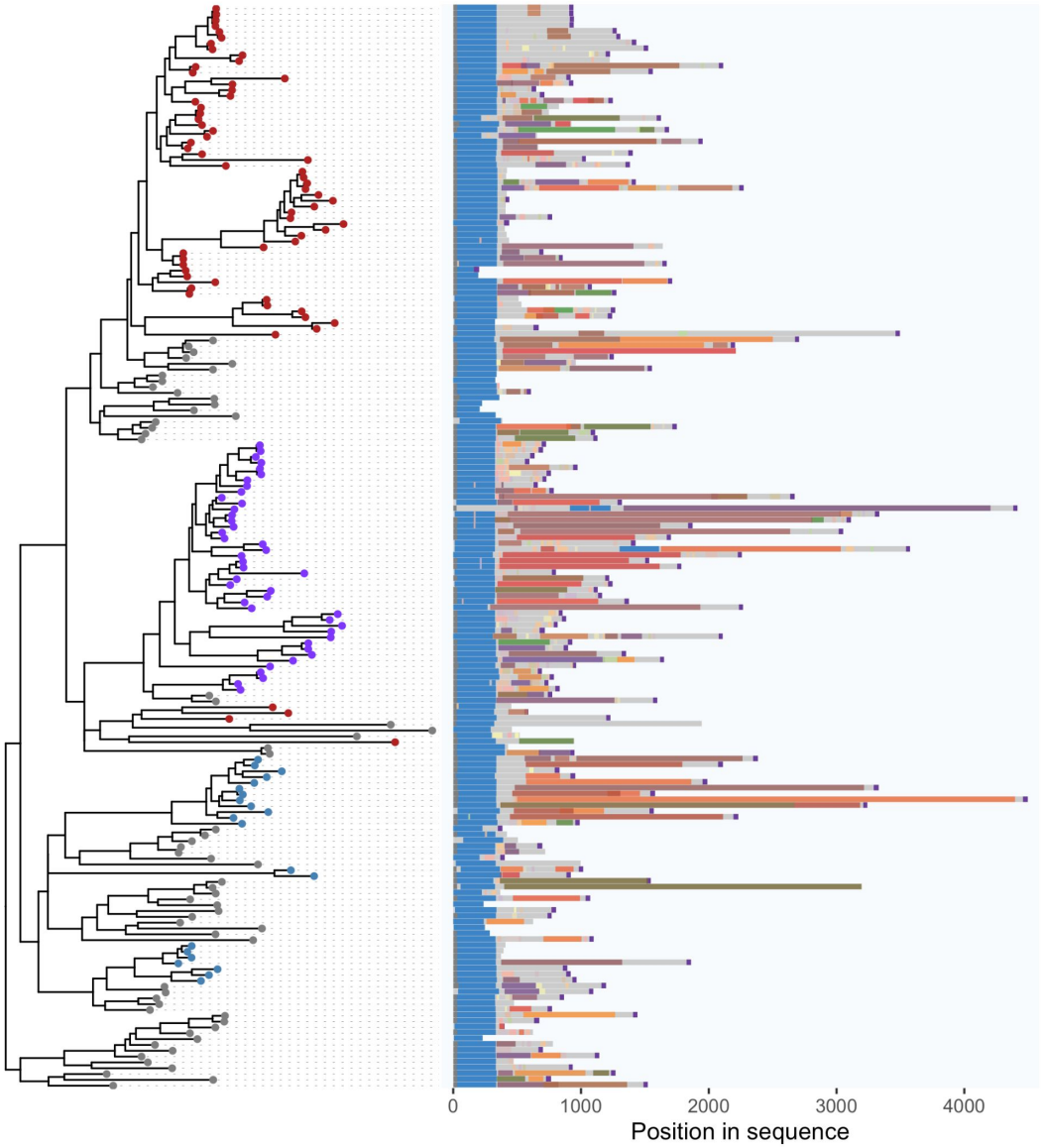

Supplementary Figure 10. Domain schematic for the Yeast Hil family showing rapidly evolving tandem repeat sequences in the central domain of the proteins. Same as Fig. 6A except that tandem repeats belonging to different sequence clusters as determined by XSTREAM (Newman and Cooper 2007) are shown in different colors.